© 2019. Published by The Company of Biologists Ltd | Development (2019) 146, dev166504. doi:10.1242/dev.166504

RESEARCH ARTICLE

Drosophila Mon1 constitutes a novel node in the brain-gonad axis that is essential for female germline maturation

Neena Dhiman[1,2], Kumari Shweta[1], Shweta Tendulkar[2], Girish Deshpande[3], Girish S. Ratnaparkhi[2,*] and Anuradha Ratnaparkhi[1,*]

ABSTRACT

Monensin-sensitive 1 (Mon1) is an endocytic regulator that participates in the conversion of Rab5-positive early endosomes to Rab7-positive late endosomes. In *Drosophila*, loss of *mon1* leads to sterility as the *mon1* mutant females have extremely small ovaries with complete absence of late stage egg chambers – a phenotype reminiscent of mutations in the insulin pathway genes. Here, we show that expression of many *Drosophila* insulin-like peptides (ILPs) is reduced in *mon1* mutants and feeding *mon1* adults an insulin-rich diet can rescue the ovarian defects. Surprisingly, however, *mon1* functions in the tyramine/octopaminergic neurons (OPNs) and not in the ovaries or the insulin-producing cells (IPCs). Consistently, knockdown of *mon1* in only the OPNs is sufficient to mimic the ovarian phenotype, while expression of the gene in the OPNs alone can 'rescue' the mutant defect. Last, we have identified *ilp3* and *ilp5* as critical targets of *mon1*. This study thus identifies *mon1* as a novel molecular player in the brain-gonad axis and underscores the significance of inter-organ systemic communication during development.

KEY WORDS: *Drosophila* oogenesis, Insulin production, Inter-organ communication, Neuronal control

INTRODUCTION

Drosophila oogenesis has served as an attractive and genetically tractable developmental model system with numerous distinguishing features (Matova and Cooley, 2001; McLaughlin and Bratu, 2015; Roth and Lynch, 2009; Spradling et al., 2001). The two prominent traits that make it simple yet unique include exquisitely detailed patterning orchestrated by the dialogue between the germline and the surrounding soma, and also fine-tuned coordination between the non-autonomous and autonomous factors that determine morphogenesis and growth (Li and Xie, 2005; Lin and Spradling, 1993; Roth and Lynch, 2009).

Drosophila adult ovary is made up of a pair of bundles, each containing 16-20 tubular structures termed ovarioles (Margolis and Spradling, 1995; Robinson and Cooley, 1997; Roth and Lynch, 2009). Each ovariole is an independent egg assembly line, comprising of six to eight egg chambers that develop in a sequential manner and are connected by stalk cells. The growth of the egg chamber is broadly divided into the previtellogenic (i.e. up to stage 8) and vitellogenic phases (i.e. beyond stage 8). The vitellogenic phase is distinguished by the exponential growth of the oocyte due to yolk accumulation. The transition from pre-vitellogenic to vitellogenic stage is under tight hormonal, as well as nutrient, control. Juvenile hormone (JH) is required for yolk formation and is necessary for vitellogenesis (Gilbert et al., 1998; Mirth et al., 2014; Raushenbach et al., 2004; Wilson, 1982); the nutritional status of the fly and the dependent growth control is regulated by insulin-like peptides (Grönke et al., 2010; Richard et al., 2005; Mirth et al., 2014; Mendes and Mirth, 2016), which also play an important role in this process. An additional layer of complexity is brought about by interactions between ecdysone-JH and insulin signaling in regulating this crucial check-point (Gruntenko and Rauschenbach, 2008, 2018; Ikeya et al., 2002; Shim et al., 2013).

Drosophila encodes eight insulin-like peptides (ILPs), of which three members (ILP2, ILP3 and ILP5) are produced by the median neurosecretory cells (MNCs) or insulin-producing cells (IPCs) (Ikeya et al., 2002). These insulin-like peptides are released into circulation through the axon terminals of the IPCs at the corpora cardiaca – a neurohemal organ (Brogiolo et al., 2001; Cao and Brown, 2001; Ikeya et al., 2002). Supporting the conclusion that ILPs exert a non-autonomous influence on the progression of oogenesis, germline-specific loss of Insulin receptor (INR) or Chico (the insulin substrate protein) leads to a reduction in the size of the ovary, an inability of the egg chambers to enter the vitellogenic stages and, consequently, sterility (Drummond-Barbosa and Spradling, 2001; LaFever and Drummond-Barbosa, 2005; Richard et al., 2005).

Previous studies in *Drosophila* have indicated that IPCs are likely to be under neuronal regulation: short neuropeptide F (sNPF) and octopamine appear to stimulate IPCs and thus can potentiate insulin signaling, whereas GABA has an inhibitory influence (Enell et al., 2010; Lee et al., 2008; Luo et al., 2014). Despite the fact that insulin signaling affects a wide variety of developmental processes in several organismal contexts, mechanisms underlying insulin production, release and transport are not fully understood. The modes of short- as well as long-range transmission have been a focus of enquiry owing to the systemic influence of insulin signaling on growth and metabolism (Erion and Sehgal, 2013; Kenyon, 2010; Partridge et al., 2011). It is generally believed that different regulatory circuits, both upstream and downstream, of insulin signaling must deploy a unique and dedicated set of regulators to achieve tissue-specific outcomes. The molecular circuitry, which participates during the synthesis and long-distance transmission of insulin, to engineer proper *Drosophila* egg chamber growth and patterning has yet to be elucidated.

In this regard, we turned our attention to a highly conserved endocytic protein, Monensin sensitive 1 (hereafter referred to as Mon1). A protein complex between Mon1, a 'longin domain'-containing protein, and CCZ1 functions as a guanine nucleotide exchange factor (GEF) for Rab7 (Nordmann et al., 2010). In a canonical endocytic cycle, Mon1 appears to be essential for the conversion of Rab5-positive early endosomes to Rab7-positive late endosomes (Nordmann et al.,

[1]Agarkar Research Institute (ARI), Pune, India. [2]Indian Institute of Science Education & Research (IISER), Pune, India. [3]Department of Molecular Biology, Princeton University, Princeton, NJ 08540, USA.

*Authors for correspondence (girish@iiserpune.ac.in; anu.aripune@gmail.com)

K.S., 0000-0002-5692-905X; G.S.R., 0000-0001-7615-3140; A.R., 0000-0001-6548-6185

Received 8 April 2018; Accepted 23 May 2019

Development (2019) 146, dev166504. doi:10.1242/dev.166504

2010; Poteryaev et al., 2010). Consequently, loss of Mon1 leads to accumulation and enlargement of early Rab5-positive endocytic compartment. In *Drosophila*, the process of Rab conversion is conserved and *mon1* is involved in the recruitment of Rab7 (Yousefian et al., 2013). Intriguingly, at the neuromuscular junction neuronal *mon1* is involved in regulating glutamate receptor levels on the post-synaptic side (Deivasigamani et al., 2015).

While characterizing the P-element mediated excision mutation in *mon1*, we noticed that homozygous mutant animals die throughout development whereas the escapers are short lived with severe motor defects (Deivasigamani et al., 2015). Recently, we also observed that *mon1* mutants display sex-non-specific sterility. Expectedly, the lethality and motor defects could be rescued by pan-neuronal expression of *mon1*. Curiously, however, the neuronal expression was also capable of rescuing the sterility in these mutants, suggesting that the neuronal expression of *mon1* may regulate fertility in wild-type females.

Here, we have analyzed mechanistic underpinnings of the influence of *mon1* on oogenesis. Our findings have uncovered an unanticipated link between neuronal *mon1* activity in octopaminergic/tyraminergic neurons (OPNs) and insulin production/signaling from the IPCs that has functional implications for the brain-gonad axis.

RESULTS

mon1 mutations influence body size and ovarian size

We have previously reported the generation of new alleles of *mon1* using P-element excision (Deivasigamani et al., 2015). Molecular characterization of one of these alleles, $mon1^{\Delta 181}$, revealed that the C-terminal region from amino acid 249 is deleted. Homozygous $mon1^{\Delta 181}$ mutants die throughout development and display motor defects (Deivasigamani et al., 2015). In addition, $mon1^{\Delta 181}$ mutant adults are ∼15% smaller in size (Fig. 1A,B) compared with wild type and exhibit sex non-specific sterility. On average, wild-type females are are 2535.82±72.27 µm (n=10) in length, whereas $mon1^{\Delta 181}$ mutant females measure 2188±97.07 µm (n=10) (Fig. 1A,B). Sterility is fully penetrant with homozygous $mon1^{\Delta 181}$ females laying very few eggs, if any.

As a first step towards understanding the underlying cause for sterility, we dissected ovaries from 2- to 3-day-old $mon1^{\Delta 181}$ mutant females. The mutant ovaries were remarkably smaller than those in

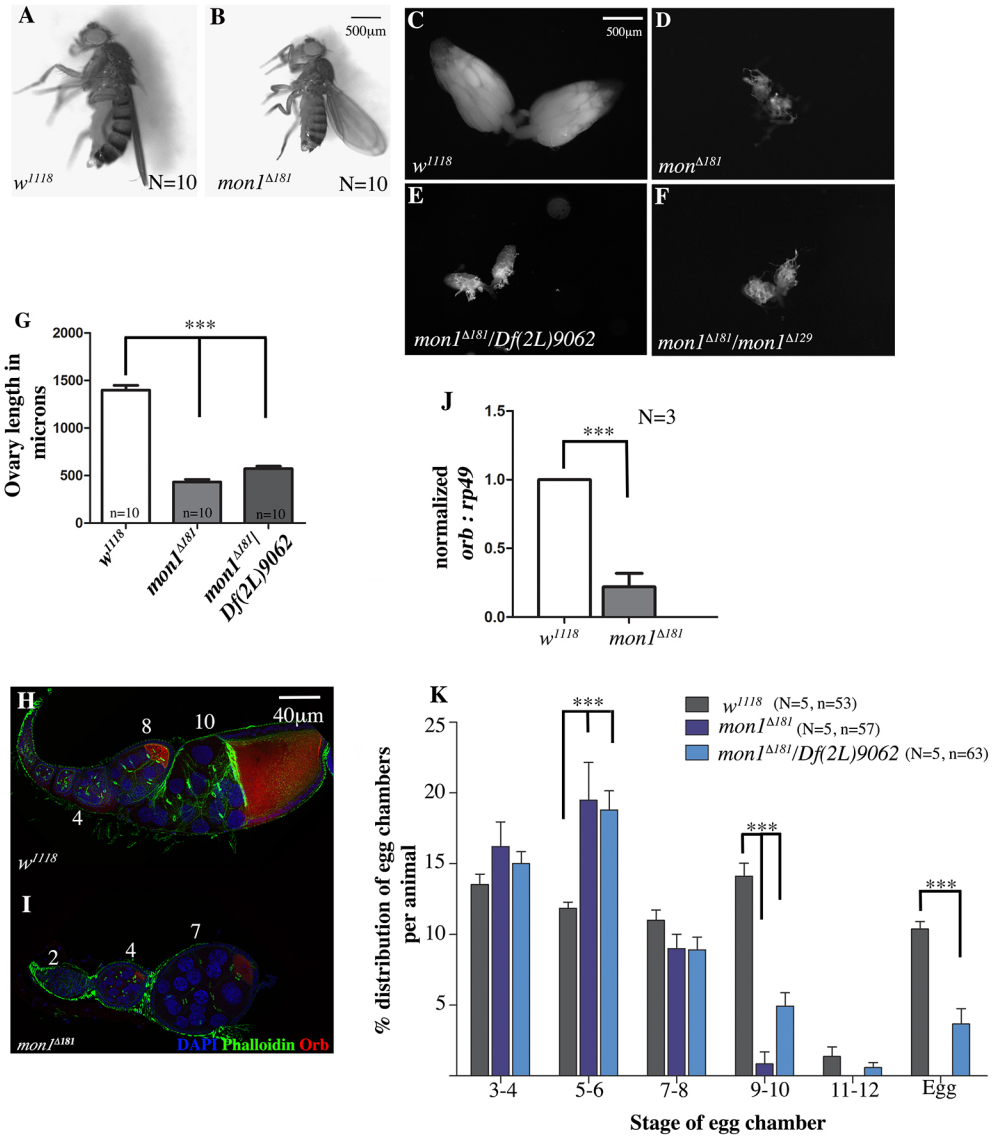

Fig. 1. *mon1* mutants have smaller ovaries with egg chambers that are stalled at pre-vitellogenic stages. (A,B) Two- to 3-day-old wild-type (A) and age-matched $mon1^{\Delta 181}$ animals. The mutant is smaller, reduced by ∼15% in length, on average, when compared with wild type. (C-F) Ovaries from 2- to 3-day-old virgin females of wild type (C), homozygous $mon1^{\Delta 181}$ (D), $mon^{\Delta 181}/Df(2L)9062$ (E) and $mon^{\Delta 181}/mon^{\Delta 129}$ (F). Mutant ovaries are extremely small compared with wild type. (G) Measurement of ovary length along the proximal-distal axis. Mutants show a ∼70% reduction in size. (H,I) Wild-type (H) and homozygous $mon^{\Delta 181}$ (I) ovarioles stained for Orb (red), and with DAPI (blue) and phalloidin (green). Late-stage egg chambers (stage 9-14) tend to be absent in *mon1* mutants (J). *Orb* transcript levels are reduced by ∼80%, with late stage egg chambers (stage 9-14) tending to be absent in $mon1^{\Delta 181}$ mutants. (K) Bar graph showing the distribution of egg chamber types from stage 3 onwards in 2- to 3-day-old w^{1118}, homozygous $mon^{\Delta 181}$ and $mon^{\Delta 181}/Df(2L)9062$ adult virgin females. Early pre-vitellogenic egg chambers predominate in the mutants. *N*=number of animals, *n*=number of ovarioles; ***P<0.001, two-way ANOVA.

Development (2019) 146, dev166504. doi:10.1242/dev.166504

control animals (Fig. 1D). To exclude the possibility that this phenotype is genetic background dependent, we also examined ovary size in *mon1*$^{\Delta 181}$*/Df(2L)9062* and *mon1*$^{\Delta 181}$*/mon1*$^{\Delta 129}$ females. *mon1*$^{\Delta 129}$ carries a small deletion that spans the C-terminal region of *mon1* and the 5′ end of the neighboring *smog* gene (Deivasigamani et al., 2015). In both cases, the ovaries were found to be very small and comparable in size with *mon1*$^{\Delta 181}$ mutants (Fig. 1E,F).

To estimate the extent of decrease in ovary size, we measured the length of the wild-type and mutant ovaries from the proximal to distal end and found that *mon1*$^{\Delta 181}$ ovaries (431.02±27.6 µm; n=10) were approximately one-third of the size of the wild-type control (1400±49.9 µm, n=10; Fig. 1G). A comparable decrease in size was also observed in ovaries from *mon1*$^{\Delta 181}$*/Df(2L)9062* adults (571.5±26 µm, n=10; Fig. 1G). Furthermore, the total number of ovarioles per animal was also significantly reduced: compared with 35.05±0.4 (n=10) in wild type, the average number of ovarioles in *mon1*$^{\Delta 181}$ mutants was reduced by ∼35% (21.3±1.13; n=5).

mon1 mutant ovaries exhibit arrested egg chamber development and partial degeneration

To assess whether different ovarian cell types (somatic as well as germline) are correctly specified, ovaries from *mon1* females were stained with DAPI, a DNA dye and fluorescently tagged phalloidin to mark actin-rich structures. We also co-immunostained these samples with antibodies against an oocyte marker, Orb. Ovaries from age-matched wild-type animals were used as controls.

The most striking phenotype seen in these mutants was the absence of late stage egg chambers (Fig. 1I). Most mutant egg chambers appeared to be arrested at pre-vitellogenic stage, with the terminal egg chamber being of stage 7 or 8 (Fig. 1I). Ten percent of the mutant ovarioles also showed degenerating terminal egg chambers (data not shown). Orb levels were also reduced compared with the control (Fig. 1H,I). Consistent with a reduction in protein levels, *orb* mRNA levels were diminished by 80% in *mon1*$^{\Delta 181}$ ovaries (normalized transcript abundance of 1 in wild-type versus 0.22±0.1 in *mon1*$^{\Delta 181}$ mutants; Fig. 1J).

The developmental arrest was quantified by plotting the percentage distribution of the egg chamber stages across ovarioles (Fig. 1K). Egg chambers counted were clubbed for two consecutive stages, e.g. stages 3 and 4 or 5 and 6 for clearer representation. In contrast to wild type (Fig. 1K), *mon1*$^{\Delta 181}$ mutants, show fewer egg chambers stage 8 onwards with a near absence of egg chambers beyond stage 9 (Fig. 1K). A similar distribution of egg chambers was observed in the ovaries from *mon1*$^{\Delta 181}$*/Df(2L)9062* with a very low proportion of ovarioles displaying late stage egg chambers and mature egg formation (Fig. 1K). Taken together, these data suggest that loss of *mon1* leads to a developmental arrest during oogenesis, resulting in the stalling of egg chamber growth at stage 7-8.

Ovary-specific knockdown of Mon1 is insufficient to recapitulate the ovarian phenotype of *mon1* mutants

For a better understanding of the developmental arrest in *mon1* mutant ovarioles, we sought to identify the cells or tissues responsible for the phenotype by reducing *mon1* transcripts in the ovary using RNAi. *mon1* expression was reduced in the germline and somatic epithelial sheath cells by using *nanos (nos)-Gal4* and *heartless(htl)*^{GMR93H07}*-Gal4* (Irizarry and Stathopoulos, 2015) drivers, respectively. In both cases, the ovaries appeared comparable in size to their respective controls, and ovarioles with mature eggs could be seen (Fig. 2A-D). The distribution of egg chambers stages in ovaries from RNAi and control animals was similar (Fig. 2E,F) suggesting that reduction of *mon1* in the ovary did not affect egg chamber development. Other ovary-specific drivers such as *E22C-Gal4* (which is expressed in both the follicle cells and germline) and maternal *alpha-tubulin*-GAL4:*VP16* (*mat-Gal4*) were also used for knockdowns and in both instances we failed to observe an effect on ovary size and egg chamber growth (Fig. S1A,B), leading us to conclude that ovarian tissue is unlikely to be the site of Mon1 action.

Downregulation of *mon1* in octopaminergic neurons leads to a decrease in ovary size and delays maturation of egg chambers

We have previously reported that pan-neuronal expression of *mon1* is able to rescue lethality as well as the neuromuscular junction phenotype induced by loss of *mon1* (Deivasigamani et al., 2015). We therefore wondered whether neuronal downregulation of *mon1* could recapitulate some aspects of the ovarian phenotype of *mon1*$^{\Delta 181}$. To test this, we expressed *UAS-mon1RNAi* in the nervous system using the pan-neuronal driver *C155*-GAL4. Surprisingly, this resulted in a significant reduction in ovary size (Fig. 2H), which was evident from the substantial increase in aspect ratio of these ovaries (compare Fig. S1C,D with Fig. S1E). We examined the distribution of egg chambers in these ovaries and found a near 50% decrease in ovarioles with mature eggs (Fig. 2K), which partially recapitulates the ovary phenotype seen in the mutants.

The ovary directly receives innervation at the ovarian peritoneal sheath muscles from the OPNs (Kurz et al., 2017; Middleton et al., 2006; Rezával et al., 2014). Knockdown of *mon1* using *tdc2*-GAL4, which expresses in OPNs (Burke et al., 2012; Erion et al., 2012), resulted in smaller ovaries (Fig. 2I,J) with an average reduction of 22% in aspect ratio compared with control ovaries (Fig. S1F). A comparison of the distribution of egg chambers in *tdc2*-GAL4>*mon1RNAi* ovaries showed a significant increase in the proportion of pre-vitellogenic egg chambers along with a near 64% reduction in mature eggs (Fig. 2L). Thus, knockdown of *mon1* in a subset of neurons (-the OPNs) seemed sufficient to partially mimic important aspects of the *mon1* mutant phenotype. This suggests that *mon1* function in OPNs is required for escaping developmental arrest. The absence of a stronger and a more complete penetrance of the mutant phenotype is likely due to inefficient knockdown of *mon1* transcript.

Expression of *mon1* in the OPNs is sufficient to rescue the ovarian defects of *mon1*$^{\Delta 181}$ mutants

These data indicate that Mon1 activity in neurons, more specifically in the OPNs, influences egg chamber maturation. We therefore examined whether the ovary phenotype was rescued in mutant animals that expressed *UAS-mon1:HA* in all neurons given that pan-neuronal expression of the transgene rescues lethality (Deivasigamani et al., 2015). Indeed, the ovaries from the rescued animals appeared normal in size (compare Fig. 3B and Fig. 1C) and displayed late stage egg chambers and mature eggs.

Next, we tested whether expression of *mon1*, in the OPNs alone, using *tdc2*-GAL4 could rescue the lethality and sterility defect in *mon1*$^{\Delta 181}$. Surprisingly, a complete rescue of lethality was observed. Although homozygous mutant flies fail to survive beyond 7 days, the ‘rescued’ females were able to live well beyond 30 days (Fig. 3E). Moreover, the morphology of the ovaries in these animals was found to be remarkably similar to wild type (Fig. 3D) and the ovariole number was also restored in these animals (35.10±0.43, n=10, w^{1118}) versus 25.30±0.84 (n=10, *mon1*$^{\Delta 181}$, *tdc2*-GAL4/*mon1*$^{\Delta 181}$) versus 34.60±0.43 (n=10, *mon1*$^{\Delta 181}$, *tdc2*-GAL4/*mon1*$^{\Delta 181}$*; UAS-mon1-HA*) (Fig. 3F).

Development (2019) 146, dev166504. doi:10.1242/dev.166504

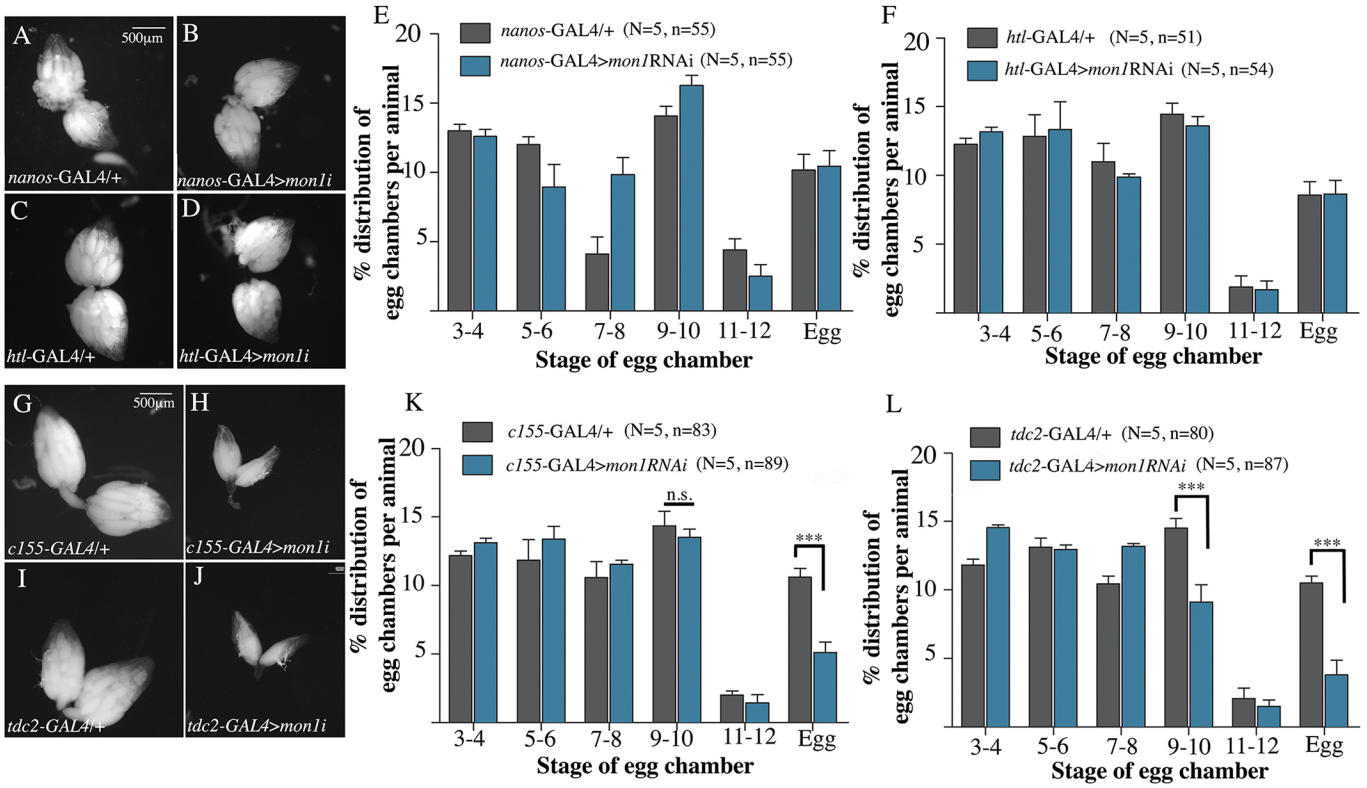

Fig. 2. Knockdown of *mon1* in OPN neurons partially phenocopies the developmental stalling seen in *mon1*$^{\Delta 181}$ ovarioles. (A-D) Downregulation of *mon1* in the germline (*nos*-GAL4>*UAS-mon1RNAi*) or sheath cells surrounding the ovary (*htl*^{GMR93H07}-GAL4>*UAS-mon1RNAi*) does not reduce ovary size or perturb gross ovarian morphology. (E,F) Distribution of egg chambers in 2- to 3-day-old *nanos*-GAL4>*UAS-mon1RNAi* (E) and *htl*^{GMR93H07}-GAL4>*UAS-mon1RNAi* (F) females is comparable with their respective controls. (G-J) Pan-neuronal (H) and *tdc2*-GAL4-specific (J) knockdown of *mon1* results in smaller ovaries compared with their respective controls (G,I). (K,L) Distribution of egg chamber types in 2- to 3-day-old *C155*-GAL4>*UAS-mon1RNAi* (K) and *tdc2*-GAL4>*UAS-mon1RNAi* (L) females along with their respective controls. Pan-neuronal knockdown of *mon1* leads to a 50% decrease in the number of mature eggs (10.61±0.62% in control versus 5.11±0.76% in RNAi animals). Expression of *UAS-mon1RNAi* in the *tdc-2* domain leads to a 37% decrease in stage 9-10 egg chambers (14.51±0.71% in control versus 9.12±1.26% in RNAi animals) and a 63% decrease in the number of eggs (10.51±0.5% in control versus 3.8±1.07% in RNAi animals). *N*=number of animals, *n*=number of ovarioles; ***P<0.001, two-way ANOVA.

We quantified the distribution of egg chambers in these animals (*tdc2*-GAL4, *mon1*$^{\Delta 181/\Delta 181}$>*UAS-mon1-HA*) and found a complete suppression of the developmental arrest: whereas in mutant females about 3% of the egg chambers are in stage 9-10, in 'rescued' females this frequency was 14% (Fig. 3G), which is comparable with wild-type control females (compare purple bar in Fig. 3G with gray bar in Fig. 1K). The ovaries of these females also showed the presence of mature eggs at a frequency of 10%, which is similar to that seen in wild-type females. A more detailed examination of the ovarioles by staining them with anti-Orb, phalloidin and DAPI showed presence of late stage egg chambers, eggs, the complete absence of degenerating of egg chambers normally seen in the mutants and the restoration of *orb* expression.

To determine the extent to which the observed rescue might be due to 'leaky' expression of the UAS transgene, we also analyzed the percentage distribution of egg chambers in *mon1*$^{\Delta 181/\Delta 181}$>*UAS-mon1:HA* animals. A minor increase in the percentage of egg chambers of stage 9-10 was observed (2.9% in *mon1*$^{\Delta 181/181}$, *tdc2*-GAL4 versus 6.82% in *mon1*$^{\Delta 181/\Delta 181}$>*UAS-mon1:HA*). These animals also showed the presence of eggs at a low frequency of 2%. However, in both cases the change did not appear to be statistically significant, indicating that 'leaky' expression is not a major contributor to the suppression of the ovary defect seen upon reconstitution of *mon1* expression in the OPNs.

We further examined the fecundity of the 'rescued' females with age-matched wild-type females by crossing each of them individually to wild-type (w^{1118}) males. Eggs laid by a single female were counted from the second day post-eclosion (Fig. 3H). Wild-type males were crossed to virgin females on the day of eclosion. Mutant *mon1*$^{\Delta 181}$ females, when mated to wild-type males, do not lay eggs. In contrast, a single wild-type female lays between 50 and 65 eggs on the second day. From the 3rd day, this number increases to an average of ∼85-95 eggs. Interestingly, the number of eggs laid by 'OPN rescue' females was comparable with wild type, with no significant difference in the number of eggs laid (Fig. 3H). In contrast, mutant females rescued using *C155*-GAL4 produced relatively fewer eggs, with the number of eggs being almost constant in the range of 65-70 after the second day. However, in both cases, as seen with wild-type females, more than 85% of the eggs were fertilized evident from the development of denticle belts. In addition, very few of these embryos hatched into first instar larvae, indicating a possible maternal requirement for *mon1* during embryogenesis. Taken together, these results suggest that expression of *mon1* in a small subset of ∼137 neurons (the OPN neurons; Pauls et al., 2018)) alone is sufficient to rescue lethality and the ovary defect in *mon1*$^{\Delta 181}$, enabling oogenesis to progress beyond the previtellogenic stages, revealing an unanticipated, yet close, functional connection between Mon1 activity and the OPNs.

Development (2019) 146, dev166504. doi:10.1242/dev.166504

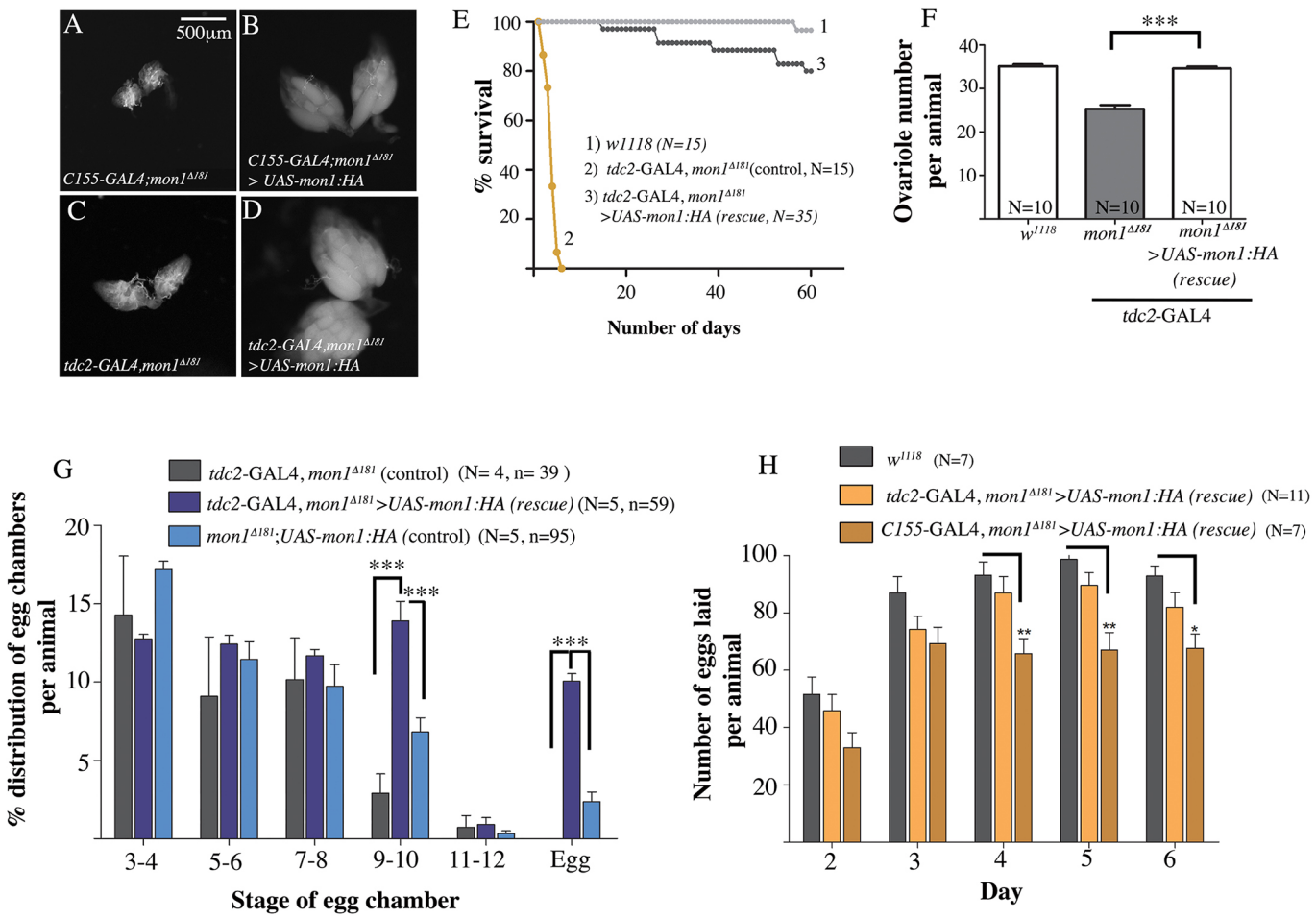

Fig. 3. Expression of *mon1* in the OPNs is sufficient to rescue lethality and ovarian defects in *mon1*$^{\Delta 181}$. (A,B) Pan-neuronal expression of *UAS-mon1:HA* using *C155*-GAL4 in *mon1*$^{\Delta 181}$ (B) rescues the 'small ovary' phenotype (A). (C,D) Expression of *UAS-mon1:HA* in a small subset of ~137 neurons, using *tdc2*-GAL4 (D, *tdc2*-GAL4, *mon1*$^{\Delta 181}$/*mon1*$^{\Delta 181}$*; UAS-mon1:HA*) also rescues the ovary phenotype in *mon1*$^{\Delta 181}$(C). (E) The short lifespan of *mon1*$^{\Delta 181}$ adults is rescued by expression of the gene in the *tdc2* domain (*tdc2*-GAL4, *mon1*$^{\Delta 181}$*>; UAS-mon1:HA*). The animals live for more than 30 days compared with the mutants that fail to survive beyond 10 days. (F) Expression of *mon1:HA* in OPNs also rescues the decrease in ovariole number observed in *mon1*$^{\Delta 181}$ animals (35±0.433 in wild type versus 21.3±1.12 in *mon1*$^{\Delta 181}$ versus 34.6±0.4 in *tdc2*-GAL4, *mon1*$^{\Delta 181}$>UAS-*mon1:HA*). (G) The 'stalling' defect in *mon1*$^{\Delta 181}$ ovarioles is rescued by expression of *mon1:HA* in the OPNs. More than a 4-fold increase is seen in the percentage of stage 9-10 egg chambers with respect to the 'GAL4' control (2.91±1.23% in mutant 'GAL4' control versus 13.9±1.24% in 'rescue') and a 2-fold increase with respect to the 'UAS' control (6.8±0.9% in 'UAS' mutant control versus 13.9±1.24% in *tdc2*-GAL4, *mon1*$^{\Delta 181}$*>UAS-mon1:HA* animals). A 10- and 5-fold increase in the number of eggs is observed with respect to the GAL4 and UAS controls, respectively (~0% in 'GAL4' control versus 2.38±0.6% in 'UAS' control versus 10.05±0.5% in *tdc2*-GAL4, *mon1*$^{\Delta 181}$>UAS-*mon1:HA* animals). (H) A comparison of the number of eggs laid per day by *w*^{1118}, *C155*-GAL4, *mon1*$^{\Delta 181}$*>UAS-mon1:HA* and *tdc2*-GAL4, *mon1*$^{\Delta 181}$>UAS-*mon1:HA* animals over 5 days. On average, wild-type and *tdc2*-GAL4, *mon1*$^{\Delta 181}$>UAS-*mon1:HA* animals are seen to lay comparable numbers of eggs, with the average number of eggs being 85-95 by the 4th day. In comparison, the number of eggs produced by *C155*-GAL4, *mon1*$^{\Delta 181}$*>UAS-mon1:HA* animals remains constant in the range of 65-70. *N*=number of animals, *n*=number of ovarioles; ***P<0.001, **P<0.01; *P<0.05; two-way ANOVA.

Expression of *Drosophila* insulin-like peptides is perturbed in *mon1* mutants

The role of insulin signaling during ovarian development in *Drosophila melanogaster* is well established (LaFever and Drummond-Barbosa, 2005) and arrested oogenesis is a hallmark of insulin pathway mutants. For example, mutations in *chico*, the substrate for insulin receptor, also cause sterility and prevent transition of the egg chambers from pre-vitellogenic to the vitellogenic phase (Richard et al., 2005) resulting in smaller ovaries.

Given the broad similarity in the ovarian phenotypes between *mon1*$^{\Delta 181}$ and insulin pathway mutants, we wondered whether *mon1* activity might target one or more of insulin-like peptides. We therefore decided to test whether endogenous insulin levels and/or signaling are compromised in *mon1* mutants. There are eight insulin-like peptides (ILPs) in *Drosophila*. As a first test, we quantitated the expression levels of these ILPs in total mRNA samples made from mutant female adults using quantitative RT-PCR. While no significant change was observed in the expression of *ilp2* and *ilp7*, a significant decrease was noted in the case of *ilp1*, *ilp3*, *ilp4*, *ilp5* and *ilp6*. Curiously, a strong increase in expression was noted for *ilp8* (Fig. 4A).

Given the significant reduction in ILP gene levels in *mon1* mutants, we wondered whether feeding the adult mutants an insulin-rich diet would ameliorate the oogenesis defects. One of the striking effects seen upon transferring newly eclosed *mon1*$^{\Delta 181}$ mutant females to medium containing 5 µg/ml of insulin (see Materials and Methods) was the improvement in their lifespan. While most homozygous *mon1*$^{\Delta 181}$ mutants die within 5 to 7 days of eclosion, mutants maintained on insulin-containing medium were able to survive for 15 days post-eclosion (Fig. 4B). We examined ovaries of

Development (2019) 146, dev166504. doi:10.1242/dev.166504

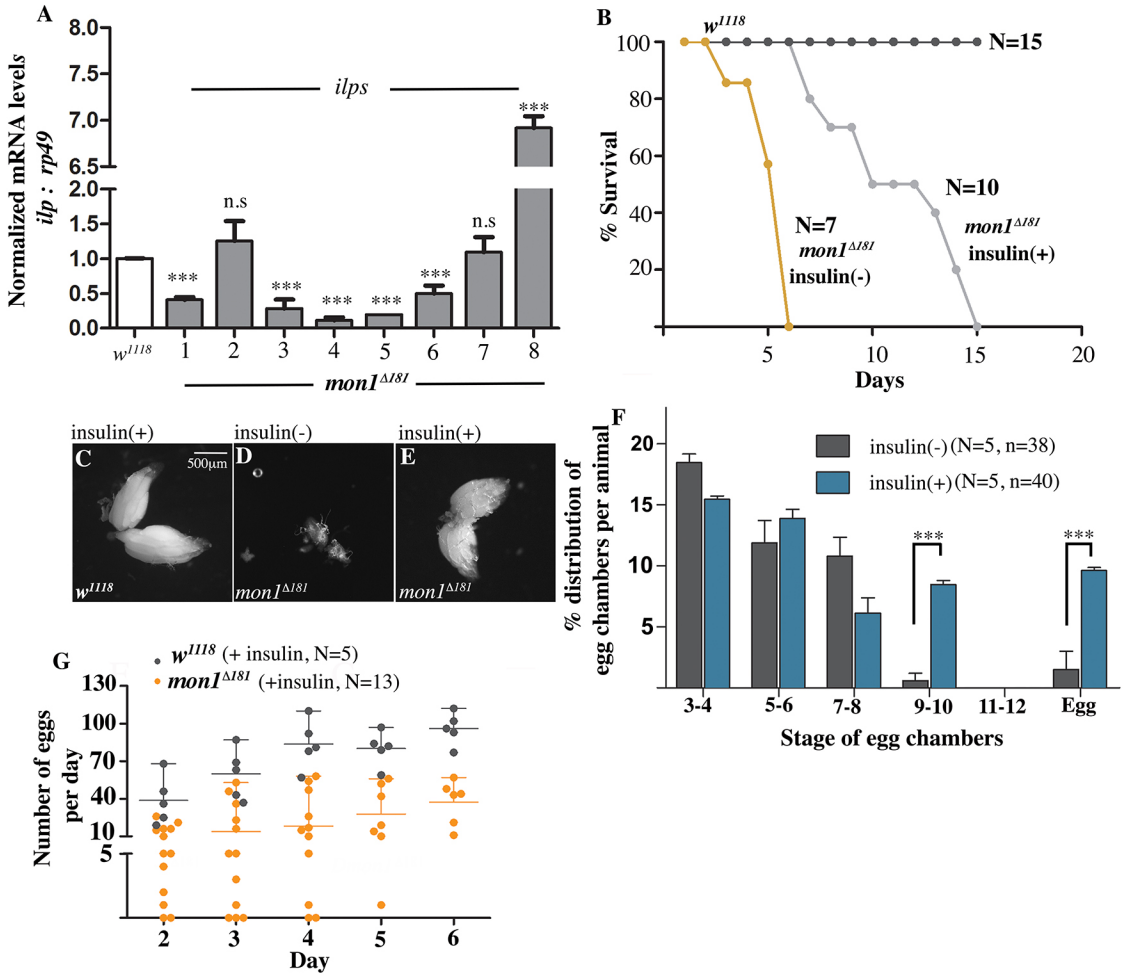

Fig. 4. Feeding insulin to *mon1*$^{\Delta 181}$ suppresses ovary defects. (A) *Ilp* mRNA levels from 2- to 3-day-old adult *mon1*$^{\Delta 181}$ whole animals normalized to wild type using quantitative real-time PCR. *ilp1*, *ilp3*, *ilp4*, *ilp5*, *ilp6* and *ilp8* show significant changes in transcript levels in the mutants. (B) Lifespan of *mon1*$^{\Delta 181}$ maintained on normal [*mon1*$^{\Delta 181}$ insulin(−)] and 5 µg/ml insulin-containing [*mon1*$^{\Delta 181}$ insulin(+)] medium. The half-life of survival is nearly doubled in animals fed on insulin-containing medium. (C-E) Five-day-old ovaries from wild type (C, insulin positive) and *mon1*$^{\Delta 181}$ flies (D,E) kept on normal (D) and insulin-containing (E) medium. Ovary size is restored in mutants fed on medium supplemented with insulin (E). (F) Percentage distribution of egg chamber stages in *mon1*$^{\Delta 181}$ [insulin(−)] and *mon1*$^{\Delta 181}$ [insulin(+)] animals. There is a significant increase in the number of stage 9-10 egg chambers [insulin(−): 0.59±0.59 versus 8.47±0.32 in insulin(+) animals] and in the number of eggs [insulin (−): 1.49±1.49 versus 9.6±0.27 in insulin(+) animals]. (G) Comparison of the number of eggs laid by *w*^{1118} and *mon1*$^{\Delta 181}$ flies fed with insulin. Each dot represents eggs laid by a single animal. *mon1*$^{\Delta 181}$ flies usually do not lay eggs. However, when kept on sucrose media supplemented with insulin, the females start laying ∼40 eggs/day by day 6, which is half the number achieved by wild-type females. *N*=number flies; *n*=number of ovarioles. ***P<0.001, two-way ANOVA.

5-day-old insulin-fed mutants with age-matched mutants maintained on normal medium. In contrast to mutant ovaries (Fig. 4D), the ovaries from the insulin-fed flies appeared to be nearly normal (Fig. 4E) in size and comparable with ovaries from wild-type animals fed on insulin (Fig. 4C). Importantly, ovarioles from insulin-fed flies displayed late-stage egg chambers (Fig. 4F). The average percentage of egg chambers at stage 9-10 in insulin-fed flies was ∼8.5% compared with 0.6% in control mutants. Similarly, the percentage of mature eggs increased dramatically to 10%, as seen in wild-type animals (see Fig. 2F), compared with 1.5% in ‘unfed’ controls.

To confirm that the effects of insulin are not due to an increase in the amount of protein in the medium, we carried out experiments in which mutant flies were separately maintained either on yeast-rich medium or on medium containing an equivalent amount of FLAG peptide (Sigma, F3290). In both cases, the ovaries appeared similar to those from mutant animals maintained on normal medium. This suggests that the suppression of the ovary phenotype in insulin-fed flies is not due to a nutrient or amino-acid rich diet but likely because of insulin activity.

To determine the physiological relevance of insulin feeding, we sought to test whether fecundity in the mutants was restored by assaying individual mutant females for their ability to lay eggs upon insulin feeding. Wild-type flies fed with insulin were used as controls. Whereas all insulin-fed *mon1*$^{\Delta 181}$ flies were able to lay eggs in their lifetime, there was considerable variation in the number of eggs laid by individual females, presumably due to variability in feeding. Moreover, because the assays were conducted on insulin-containing sucrose agar medium, 60% of the mutant females failed to survive beyond the third day. Nonetheless, about 20% of the flies were able to produce, on an average, more than 35 eggs per day, with some females laying as many as 40 eggs (Fig. 4G). Furthermore, 80% of the eggs laid appeared to be fertilized, based on development of cuticular structures. The observation that feeding insulin is able to alleviate both the morphological aberrations and the functional defects suggests that the effect of insulin on ovarian

Development (2019) 146, dev166504. doi:10.1242/dev.166504

growth is not simply a result of an 'insulin-dependent bypass'. These data thus argue that the insulin pathway is likely a physiologically relevant target of *mon1* activity.

ILP5 levels are considerably reduced in *mon1* mutant IPCs

The transcript levels of a number of ILPs are reduced in *mon1* mutants (Fig. 4A). Taken together with the observation that an insulin-rich diet can partially suppress the ovarian phenotype, we wondered whether *mon1* influences ILP levels. We therefore examined whether *mon1* is specifically necessary to maintain ILP levels in the IPCs. IPCs synthesize ILP2, ILP3 and ILP5 but only *ilp3* and *ilp5* mRNA levels are reduced in *mon1* mutants. As *ilp5* has been shown to influence oogenesis (Badisco et al., 2013; Richard et al., 2005), we decided to examine the level of ILP5 in IPCs by staining the adult brains using anti-ILP5 antibodies. Compared with wild type, a substantial decrease in ILP5 levels was observed in $mon1^{\Delta 181}$ IPCs and in the axons projecting from these cells (compare Fig. 5A with 5B,C). In some animals, the decrease was very dramatic, with IPCs displaying ILP5 staining only at the periphery (Fig. 5C) of the cell body. We quantified the intensity of ILP5 staining in the IPCs and compared it with the levels in the heterozygous mutant and wild-type animals. In both cases, a 50-60% decrease in ILP5 intensity was observed. Given the association between Mon1 and the OPNs in the context of ovary maturation (Fig. 2), we wondered whether knockdown of *mon1* in the OPNs might affect ILP5 levels. Interestingly, expression of *mon1* RNAi in OPNs led to a significant decrease in ILP5 staining in the IPCs as well as the projecting axons (compare Fig. 5E with 5F). Curiously, the staining in the RNAi animals appeared punctate. A quantification of the staining intensity showed a 40% decrease in RNAi animals compared

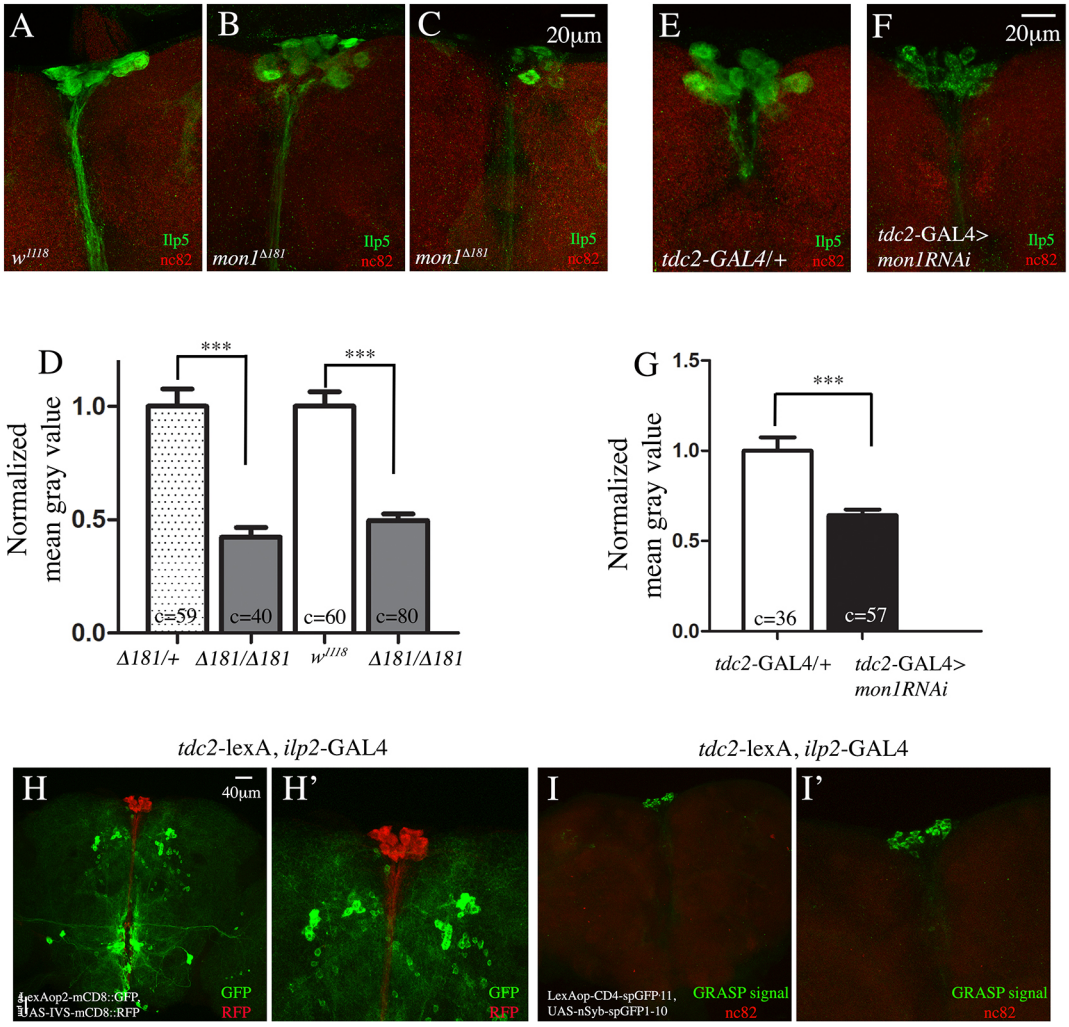

Fig. 5. *mon1* in OPNs regulates *ilp5*, and OPNs make direct synaptic connections with the IPCs. (A-C) Adult brains of w^{1118} (A) and $mon1^{\Delta 181}$ mutants (B,C) stained using anti-ILP5 (green) and anti-Brp (red) antibodies. There is a distinct decrease in the intensity of ILP5 staining in the mutants (B,C). In a few cases, the IPCs exhibit only faint staining around the edge of the cells (C). (D) Quantification of the staining intensity shows, on average, a 50% reduction in staining intensity between control and mutants [$mon1^{\Delta 181/+}$, 1.0±0.07 (*c*=59 cells, *N*=6) versus 0.43±0.04 (*c*=40 cells, *N*=6) in $mon1^{\Delta 181}$; w^{1118}, 1.0±0.06 (*c*=60 cells, *N*=6) versus 0.49±0.3 (*c*=80 cells, *N*=7) in $mon1^{\Delta 181}$]. (E-G) Adult brains of *tdc2*-GAL4/+ (E) and *tdc2*-GAL4>*UAS-mon1RNAi* (F) stained using anti-ILP5 (green) and anti-Brp (red) antibodies. Intensity of ILP5 staining in the IPCs is reduced in upon downregulation of *mon1* in OPNs (compare F with E). (G) The decrease in intensity is ∼40% [*tdc2*-GAL4/+, 1.00±0.07 (*c*=36, *N*=5) versus 0.63±0.03 (*c*=57 cells, *N*=8) in *tdc2*-GAL4>*UAS-mon1RNAi*]. (H,H′) Adult brain of a *tdc2*-lexA, *ilp2*-GAL4>lexAop-mCD8GFP, UAS-IVS-mCD8::RFP animal stained using anti-GFP (green) and anti-RFP (red) antibodies. The organization of the two sets of neurons is shown (H). A more detailed image of H is shown in H′. (I,I′) Adult brain of a *tdc2*-lexA, *ilp2*-GAL4>LexAopCD4-spGFP11, UAS-nSyb-spGFP1-10 animal. Localized GFP staining representing the GRASP signal is seen at the IPCs alone (I). A more detailed image of I is shown in I′.

Development (2019) 146, dev166504. doi:10.1242/dev.166504

with controls (Fig. 5G). Thus, both *ilp5* mRNA and protein levels are lowered in *mon1* mutants and knockdown of *mon1* in OPNs alone is sufficient to decrease the level of ILP5 in the IPCs.

Based on the proximity of the dendrites of the IPCs and the OPNs, it has been speculated that these neurons may form direct synaptic connections with each other (Luo et al., 2014). Given the non-autonomous regulation of *ilp5* by Mon1, we decided to test whether IPCs and OPNs form synaptic connections using the 'GFP resonstitution across synaptic partners' (GRASP) technique in which two membrane-bound complementary split fragments of GFP are expressed independently in two neuronal cell types to reconstitute a functional GFP at synaptic sites (Feinberg et al., 2008). To achieve this, we recombined the *tdc2*-LexA driver with *ilp2*-GAL4. We confirmed the presence of both drivers by crossing the recombinant line with GFP and RFP reporters for GAL4 and LexA, respectively (Fig. 5H,H′). Interestingly, when crossed to a line carrying the split-GFP reporters for LexA and GAL4, reconstituted GFP or GRASP signal was detected only at the IPCs (Fig. 5I,I′), indicating that the OPNs make direct synaptic contacts with the IPC cell body. This observation strongly suggests that the regulation of *ilp5* by Mon1 in the OPNs is likely to be direct.

Overexpression of *ilp5* or *ilp3* in IPCs can alleviate loss of *mon1*

Based on the above results, we sought to assess whether the reduction in ILP5 levels in *mon1* mutant IPCs is an important factor that contributes to its ability to regulate egg chamber maturation. If so, we expected neuronal expression of ILP5 to mitigate the ovarian phenotype due to loss of *mon1*. Consistent with this, expression of *UAS-ilp5* using a pan-neuronal driver (*C155-Gal4*; compare Fig. 6A,B) or an IPC-specific driver (*ilp2-Gal4*; compare Fig. 6C with D) was able to ameliorate the ovary phenotypes of $mon1^{\Delta 181}$. With both drivers, nearly 50% of the mutant animals showed near wild-type-like ovaries, while others showed a partial rescue in which ovaries were bigger than $mon1^{\Delta 181}$ mutants but with relatively fewer eggs. Furthermore, overexpression of *ilp5* in the IPCs was able to restore ovariole number in the mutants (31.67±1.2, n=6). Improved viability was evident from the increase in frequency of obtaining mutant flies.

We compared the distribution of egg chambers between individual animals expressing *UAS-ilp5* and *UAS-mon1HA* under the pan-neuronal *C155*-GAL4. As expected, the latter showed substantial increase in the number of late-stage egg chambers and eggs. Expression of *ilp5* also led to an increase in the percentage of late-stage egg chambers and eggs, albeit to a lesser extent compared with *UAS-Mon1HA* (Fig. 6E).

In addition to ILP5, IPCs are known to synthesize ILP2 and ILP3. Previous studies have indicated existence of partial redundancy among the different ILPs (Broughton et al., 2008; Grönke et al., 2010). We examined whether pan-neuronal or IPC-specific overexpression of *ilp2* and *ilp3* could achieve an analogous rescue of the ovary phenotype in $mon1^{\Delta 181}$. Overexpression of *ilp2* did not yield viable adults. In contrast, overexpression of *ilp3* using *C155*-GAL4 suppressed the ovary defect in a manner comparable with *ilp5* in terms of the ovariole number as well as relieving the egg chamber arrest (Fig. 6E). Similar to expression of *ilp5*, improvement in viability was evident from the increase in frequency of getting mutant adults.

Further supporting these results, overexpression of *ilp5* and *ilp3* in the IPCs alone was sufficient to suppress the egg chamber arrest. As with pan-neuronal expression, the overall ovarian morphology in 50% of the animals resembled wild type whereas in the others, the rescue was partial with an appreciable increase in the number of late-stage egg chambers and eggs (Fig. 6F). Overexpression of *ilp5* and *ilp3* in the OPNs was unable to suppress the loss of viability and ovarian defects in the mutants, thus confirming the IPC-specific role of *ilp5* and *ilp3* (data not shown).

To determine whether expression of *ilp3* and *ilp5* also rescued fecundity, we assayed the ability of mutant females to lay eggs by individually crossing them to wild-type males. Indeed, these females were able to lay eggs and more than 75% of these eggs were fertilized (Fig. S2). An observation made during these egg-laying assays was the increase in mortality of mutant flies when placed on sucrose agar medium when compared with regular corn-meal agar medium, indicating increased sensitivity to nutrition. In summary, neuronal expression of both *ilp5* and *ilp3* in *mon1* mutant females was able to relieve the egg-chamber arrest during oogenesis, leading to restoration of the normal physiological function of the ovary. The partial nature of the rescue suggests presence of additional Mon1 targets or the requirement for combinatorial ILP expression. Future studies will focus on identification and characterization of these novel molecular players.

DISCUSSION

ILPs, in conjunction with the insulin receptor are involved in a variety of conserved biological processes that ultimately impact growth advantage, developmental profile, reproductive potential and aging-dependent decline (Boulan et al., 2015; Richard et al., 2005; Shim et al., 2013). Recent data also suggest that insulin can affect behavioral traits via nervous system function and physiology (Graham and Pick, 2017; LaFever and Drummond-Barbosa, 2005).

In *Drosophila*, differential expression of the ILPs and the systemic nature of their function underlie their diverse spatiotemporal roles (Bai et al., 2012; Grönke et al., 2010; Gruntenko and Rauschenbach, 2018; Hsu and Drummond-Barbosa, 2009; Knoblich, 2012; Richard et al., 2005; Shim et al., 2013; Ueishi et al., 2009). Emphasizing the importance of the long-distance nature of its communication and regulation, elegant studies by Rajan and Perrimon have demonstrated that Unpaired2 (Upd2) secreted by the fat body communicates with the IPCs to induce secretion of ILPs for maintenance of metabolic homeostasis (Rajan and Perrimon, 2012). A subsequent study from the Leopold lab has shown GPCR signaling by Methuselah (Mth) in response to Stunted (Sun) regulates secretion of ILPs (Delanoue et al., 2016). Regulation of insulin signaling during organ development and maturation has been studied extensively in the context of oogenesis and its role in regulating vitellogenesis is well established. In this study, we show that Mon1, an endocytic factor, regulates ovary maturation by participating in a non-autonomous mechanism to control expression of ILPs in the IPCs.

mon1 mutants display female sterility; the mutant females have small ovaries with fewer ovarioles. The individual mutant egg chambers are arrested at the previtellogenic stages, resulting in ovaries that are devoid of any mature eggs. Interestingly, *mon1* activity appears to be required not in the ovaries, but in the nervous system. Supporting such a non-cell autonomous control by Mon1, compromising *mon1* levels specifically in the OPNs appears sufficient to induce developmental stalling at the vitellogenic checkpoint.

The observation that expression of *mon1* using a pan-neuronal driver is sufficient to rescue both lethality and sterility strongly supports a neural basis for the *mon1*-dependent defects. That expression in the approximately 176 OPNs labeled by *tdc2*-GAL4 in the brain and ventral ganglion (Pauls et al., 2018) is sufficient to rescue both lethality and sterility in these mutants argues that these might be the functionally crucial subset in this regard.

Development (2019) 146, dev166504. doi:10.1242/dev.166504

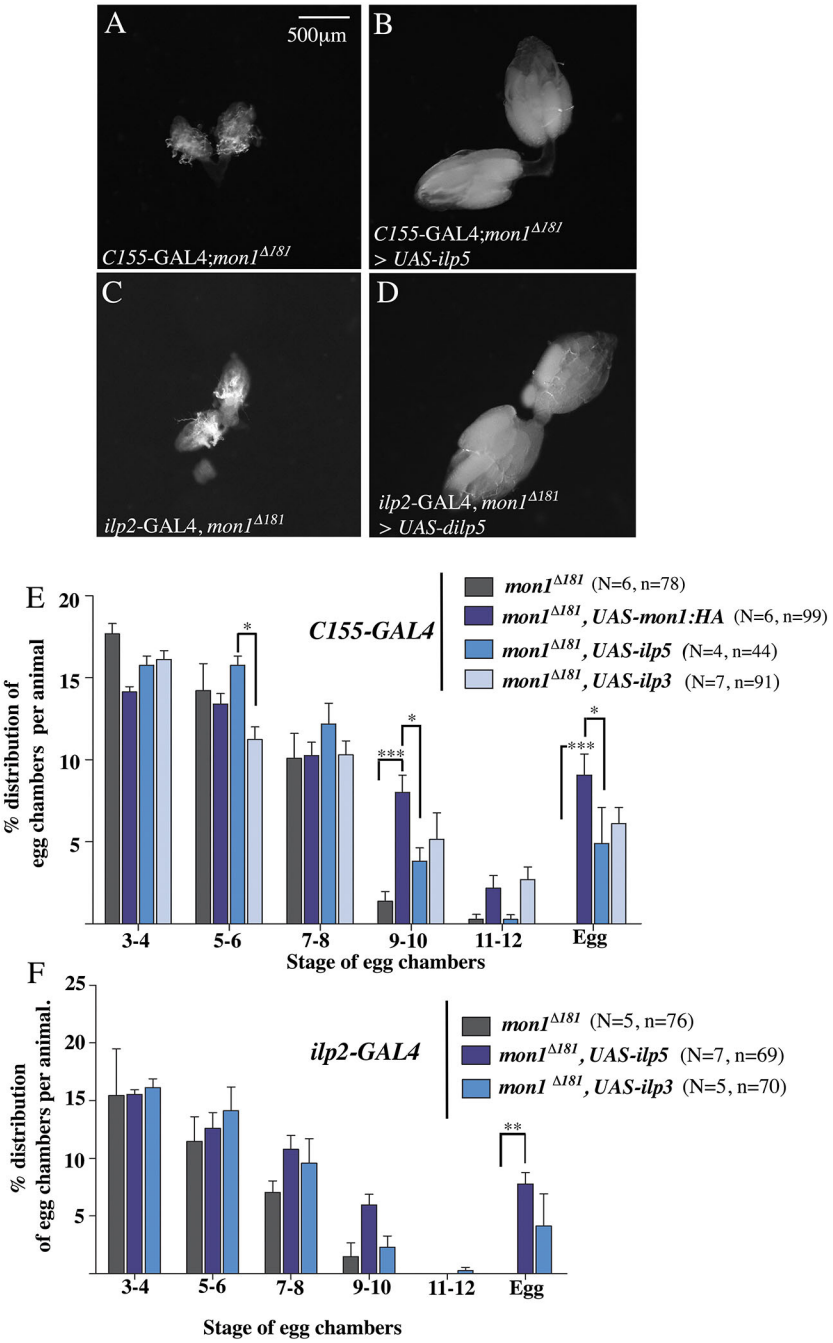

Fig. 6. Expression of *ilp5* and *ilp3* rescues the egg-chamber stalling defect in *mon1*$^{\Delta 181}$ mutants. (A,B) Pan-neuronal expression of *ilp5* (*C155*-GAL4; *mon1*$^{\Delta 181}$*>UAS-ilp5*) rescues ovary size in *mon1*$^{\Delta 181}$ mutants (compare A with B). (C,D) Expression of *ilp5* in IPCs using *ilp2*-GAL4 (*mon1*$^{\Delta 181}$, *ilp2*-GAL4/*mon1*$^{\Delta 181}$, *UAS-ilp5*) rescues ovary size in *mon1* mutants (compare C with D). (E) A comparison of the percentage distribution of egg chambers between control (*C155*-GAL4; *mon1*$^{\Delta 181}$) and mutants expressing *UAS-Mon1:HA*, *UAS-ilp5* and *UAS-ilp3*. A significant increase in the number of egg chambers at stage 9-10 is observed upon expression of *UAS-mon1:HA* (mutant control: 1.37±0.59 versus 8.07±1.04 in *C155*-GAL4; *mon1*$^{\Delta 181}$*>UAS-mon1:HA*). A smaller increase is seen with *UAS-ilp5* (3.82±0.81) and *UAS-ilp3* (5.15±1.61). A significant increase in the number of eggs is seen in all three genotypes (*mon1*$^{\Delta 181}$: 0 versus 9.07±1.28 in *C155*-GAL4; *mon1*$^{\Delta 181}$*>UAS-mon1:HA* versus 4.9±2.19 in *C155*-GAL4; *mon1*$^{\Delta 181}$*>UAS-ilp5* versus 6.11±0.99 in *C155*-GAL4; *mon1*$^{\Delta 181}$*>UAS-ilp3*). (F) Distribution of egg chamber stages in mutants expressing *UAS-ilp5* and *UAS-ilp3* in the IPCs. Note the increase in the number of stage 9-10 egg chambers [1.47±1.21 (mutant control) versus 5.95±0.93 (*ilp2*-GAL4; *mon1*$^{\Delta 181}$*>UAS-ilp5*) versus 2.3±0.94 (*ilp2*-GAL4; *mon1*$^{\Delta 181}$*>UAS-ilp3*)] and mature eggs [0 (mutant control) versus 7.78±0.98 (*ilp2*-GAL4; *mon1*$^{\Delta 181}$*>UAS-ilp5*) versus 4.14±2.76 (*ilp2*-GAL4; *mon1*$^{\Delta 181}$*>UAS-ilp3*)]. *P<0.05; **P<0.01; ***P<0.001; Student's *t*-test was used to compare intensity of ILP5 staining. Egg chamber distribution (E,F) was analyzed using two-way ANOVA. *N*=number of animals, *n*=number of ovarioles.

Given that the sterility and ovarian phenotypes seen in *mon1* mutants are reminiscent of those seen in *chico* mutants that have impaired insulin signaling, we checked for a possible connection between *mon1* and insulin signaling. Two findings are of interest in this context. First, levels of a number of ILP genes (*ilp1*, *ilp3*, *ilp5* and *ilp6*) are significantly reduced in *mon1*$^{\Delta 181}$ mutants. Second, feeding an insulin-rich diet to homozygous *mon1*$^{\Delta 181}$ females ameliorates the ovarian phenotypes induced by the loss of *mon1* (Fig. 4).

Our data show that knockdown of *mon1* in the OPNs regulates ILP5 levels in the IPCs, pointing towards a non-cell-autonomous mode of regulation of ILP levels (Fig. 5). Furthermore, our results from the GRASP experiments show that OPNs make direct synaptic connections with the IPCs, suggesting that the regulation by Mon1 is likely to be direct between the two cell types (Fig. 5). Taken together, our results suggest that Mon1 in OPNs is required to control production and/or secretion of ILPs in the IPCs.

The octopamine receptor OAMB is expressed in the IPCs and its knockdown has been shown to increase *ilp3* mRNA levels with no effect on *ilp2* and *ilp5* in the IPCs (Luo et al., 2014). This is in contrast to *mon1* mutants that show reduced levels of *ilp3* and *ilp5*, but not *ilp2*. The mechanism by which Mon1 regulates ILP expression and whether the circulating levels of the respective ILPs are also affected in a consistent manner still remains to be determined.

Our genetic analysis indicates that expression of ILP2 in the IPCs is not sufficient to rescue the lethality and ovarian phenotype in *mon1* mutants. Consistent with this, we found ILP2 levels to be elevated (Fig. S3), possibly in response to low levels of other ILPs. Altogether, our results argue that *mon1* functions in the OPNs in a manner that places it genetically upstream of insulin signaling to regulate ovary

Development (2019) 146, dev166504. doi:10.1242/dev.166504

maturation. Elucidating the mechanistic underpinnings of this regulatory relationship will be the focus for future studies.

It is remarkable that, in context of the neuromuscular junction, *mon1* appears to be secreted by the presynaptic terminals (Deivasigamani et al., 2015). This observation suggests that it is competent to function in a non-cell-autonomous manner. As in the case of the neuromuscular junction, it is possible that Mon1 engineers the expression of OAMB or other octopamine receptors, thereby indirectly influencing the activation of IPCs. Alternatively, Mon1 may facilitate the release of as yet unknown factors that influence expression of ILPs. These possibilities need to be explored by directly testing the levels and/or activity of OAMB receptors and ILPs in the IPCs.

Secretion of ILPs is thought to be regulated by ecdysone and juvenile hormone. The IPC/JH axis is part of an integrated network that regulates spatiotemporal growth and development in the fly. The interdependence of signaling of elements in the network, the presence of positive- and negative-feedback loops and the context dependence suggests that both the JH and DILPs are important players in the pre-vitellogenic checkpoint. We therefore tested whether Mon1 exerts its influence on oogenesis via these pathways. Arguing against the possibility, however, feeding $mon1^{\Delta 181}$ mutant flies with 20-OH ecdysone did not rescue the ovarian phenotype to any appreciable extent. Topical addition of JH led to a mild rescue of the $mon1^{\Delta 181}$ phenotype to about 15% of that of wild-type flies. In contrast, feeding excess levels of insulin effectively rescued the $mon1^{\Delta 181}$-dependent ovarian phenotype to about 70% of wild type. Furthermore, the extent of rescue could be correlated with the amount of insulin intake and the length of feeding time. For example, mutant flies fed on insulin-containing medium for 10 days show a near complete rescue of the ovarian phenotypes, including rescue of the ovariole number and presence of mature eggs. A similar rescue is seen at day 5, although these ovaries tend to have a few ‘mutant-like’ small ovarioles. Taken together, these observations strongly suggest that defects induced by the loss of Mon1 are, at least in part, due to impaired insulin signaling. Consistently, phospho-4EBP1 levels for whole-fly lysates are ∼45% reduced in $mon1^{\Delta 181}$ mutant flies (Fig. S4).

OPNs, to date, have not been implicated in ovarian development. Our data suggest that ILP3 and ILP5, but not ILP2 regulate the vitellogenic checkpoint and the production of ILPs in IPCs is, in turn, regulated by an unknown signal emanating from the OPNs. Mon1 in OPN neurons appears to function as a crucial node for activating this signal and thus regulates ILP3/ILP5 levels, adding an additional level of control for insulin signaling under normal feeding conditions, i.e. in the absence of starvation.

Our data reveal a novel regulatory loop involving a specific subset of neurons and insulin metabolism that, in turn, results in phenotypic abnormalities at the organismal level. Although the precise identity of the individual effectors is unclear at present, these data clearly demonstrate how systemic level communication between individual cells, tissues and even organs can participate in, and contribute to, organismal homeostasis.

MATERIALS AND METHODS

Fly husbandry and strains used

All stocks were reared on standard corn meal agar medium. $mon1^{\Delta 181}$ and $mon1^{\Delta 129}$ were generated through excision of pUAST-Rab21::YFP insertion using standard genetic methods (Deivasigamani et al., 2015). *Df(2L)9062, C155*-GAL4, *tdc2*-GAL4 (#9313), *htl*-GAL4^{GMR93H07} (#40669) and *nos*-GAL4 are from the Bloomington Stock Center. The *mon1* RNAi line (GD7852) is from the VDRC stock center. Other stocks were as follows: *UAS-mon1::HA* (a kind gift from T. Klein, University of Dusseldorf, Germany), *ilp2*-GAL4 (Rulifson et al., 2002), *UAS-ilp5* and *UAS-ilp3* (G. Hasan, NCBS, Bangalore; Ikeya et al., 2002); *tdc2-LexA::p65* (#52242, Bloomington Stock Center); *UAS-nSyb-spGFP1-10*, *LexAop-CD4-spGFP11* (# 64314, Bloomington Stock Center); and *10XUAS-IVS-mCD8::RFP*, *13X LexAop2-mCD8::GFP* (# 32229, Bloomington Stock Center). Except when stated, all crosses were carried out at 25°C.

Immunostaining and imaging

For whole-ovary imaging, adult ovaries were dissected in 1× PBS at 4°C, and imaged using an Olympus Axio Zoom Stereoscope. All images were taken at the same magnification. For immunostaining, adult ovaries were dissected in 1× PBS at 4°C and fixed with 4% paraformaldehyde in 1× PBS with 0.3% Triton-X for 25 min at room temperature. The samples were washed six times in 1× PBS with 0.3% Triton-X for 15 min each and blocked in 2% BSA and 0.3% Triton-X in 1× PBS for 1 h. Incubation with primary antibody was carried out overnight at 4°C. Post-primary antibody incubation, the samples were washed four times for 10 min in 1× PBS containing 0.3% Triton-X and incubated with the appropriate fluorescent secondary antibody for 1 h at room temperature in the dark. The ovaries were then washed (six times for 5 min each in PBST) and mounted using 70% glycerol containing n-propyl gallate. A pair of ovaries from a single adult female was mounted per coverslip to count the number of ovarioles and to determine the proportion of different egg chambers per ovariole. The concentrations of the different dyes and antibodies were as follows: DAPI [Thermo-Fisher (Molecular Probes), D1306, 1:500]; phalloidin 488 [Thermo-Fisher (Molecular Probes), A12379, 1:100]; anti-Orb (DSHB, 1:20); Alexa Fluor secondary antibodies [Thermo-Fisher (Molecular Probes), A11031, A11034; 1:1000]. Imaging was carried out using the Leica SP8 confocal microscope system with a 40× oil objective (1.3 N.A.). Immunostaining of adult brains was carried out as described previously (Pfeiffer et al., 2010). Anti-ILP5 and anti-ILP2 (1:800 and 1:400 respectively; kind gifts from P. Leopold, Institut Curie, France). Image processing and intensity measurements were done using ImageJ software (NIH). The image of the ovary in Fig. 1H was created from two overlapping pictures and assembled by merging them in Photoshop to obtain the image of the entire ovariole. For the GRASP experiment (Fig. 5I), GFP staining was carried out using anti-chicken GFP (Thermo-Fisher, A10262, 1:1000). Identical staining was obtained with anti-rabbit GFP (Thermo-Fisher, A11122, 1:1000; Kim et al., 2012; Zhou et al., 2015) and anti-RFP (a kind gift from R. Hegde, Cambridge, UK; 1:2000). GraphPad Prism was used for statistical analyses. All data are presented as mean±s.e.m. Figures were assembled using Adobe Photoshop CS4.

Quantitative RT-PCR

Estimation of *orb* levels was carried out using quantitative PCR on cDNA synthesized from mRNA isolated from adult wild-type (w^{1118}) and *mon1* mutant ovaries. The ovaries were dissected in ice-cold 1× PBS. RNA isolation was carried out using Trizol reagent according to the manufacturer’s instructions. For estimation of ILPs, mRNA was isolated from 1- to 2-day-old adult female flies. In each case, 1 µg of RNA was used for the reverse transcription reaction. The sequence of the primers used for quantitative PCR are as follows: *rp49-f*, GACGCTTCAAGGGACAGTATC; *rp49-r*, AAACGCGGTTCTGCATGAG; *orb-f*, GAGTGGGAAAGGGAAGGTAC; *orb-r*, CAGGTAGGAGCTTATCGAGTG; *ilp1-f*, GGTGTGTCCCCATGGCTTTA; *ilp1-r*, TGCTGCTATCATCCTGCACC; *ilp2-f*, CGAGGTGCTGAGTATGGTGTG; *ilp2-r*, CCCCAAGATAGCTCCCAGGA; *ilp3-f*, ATGGGCATCGAGATGAGGTG; *ilp3-r*, CGTTGAAGCCATACACACAGAG; *ilp4-f*, ATGAGCCTGATTAGACTGGGAC; *ilp4-r*, TCTAGCATCCTTAGACGCACT; *ilp5-f*, TGCCTGTCCCAATGGATTCAA; *ilp5-r*, GCCAAGTGGTCCTCATAATCG; *ilp6-f*, GTCCAAAGTCCTGCTAGTCCT; *ilp6-r*, TCTGTTCGTATTCCGTGGGTG; *ilp7-f*, AGGAGGGTCTCGAGATGCTT; *ilp7-r*, CCCAATATAGCTGGCGGACC; *ilp8-f*, GGACGGACGGGTTAACCATT; and *ilp8-r*, CATCAGGCAACAGACTCCGA.

Feeding experiments

Regular corn-meal medium was supplemented with 5 µg/ml of bovine insulin (Sigma-Aldrich, I6634). Newly eclosed wild-type and $mon1^{\Delta 181}$

mutant females were transferred to insulin-containing medium. Ovaries were examined in 5-day-old animals. For measurement of life span, the animals were maintained on insulin medium for the entire duration of the experiment. For comparison of feeding behavior of $mon1^{\Delta 181}$ with wild-type flies, we used a food dye (Brilliant Blue FCF, Sigma 80717). Animals are starved for 4 h and fed on either 0.5% sucrose-soaked filter paper or corn-meal agar for 1 h. In both cases, 0.5% dye is incorporated in the nutrient medium. The amount of dye intake was measured by spectrophotometry (λ629, Varioscan plate reader) for eight animals (N=3 experiments) in fly lysates that were homogenized in water and centrifuged for 15 min at 14,000 ***g***. Two-day-old $mon1^{181}$ adults appeared to ingest equal amounts of food/sucrose when compared with age-matched $mon1^{181}$/+ or w^{1118} adults.

Application of Juvenile hormone

Acetone was used as a vehicle to dissolve and apply Juvenile hormone (JH) III (J2000, Sigma). One-day-old adult flies were topically administered JH by pipetting 0.5 µl of solution onto the abdomen of the fly. JH was applied at the concentrations of 0.1, 1 and 5 µg per animal. The concentrations used were consistent with the range used in earlier studies (Gruntenko et al., 2019; Rauschenbach et al., 2014; Terashima and Bownes, 2004). The animals were kept on yeasted corn-meal agar for 48 h before dissection of ovaries and counting of the number of eggs (stage 13-14) per animal. There was an increase in the number of eggs (stage 13-14) from <1 per animal ($mon1^{\Delta 181}$) to 4.77±2.0 eggs per animal in response to JH application when compared with wild-type animals (33±3.2 eggs per animal).

Analysis of egg chamber distribution

All analysis to determine the distribution of egg chambers was carried out on 2- to 3-day-old virgin females maintained on regular cornmeal agar medium containing yeast soon after eclosion. The number of egg chambers for each stage were scored on a ‘per animal’ basis. Except where stated, the data presented for each stage is an average for 5 animals (n=5).

Fecundity assay

Individual newly eclosed virgin females of the appropriate genotype were crossed to single w^{1118} males and transferred on the same day to a sucrose agar medium containing a small amount of yeast paste. Sucrose plates were changed every 24 h. The day of eclosion was treated as ‘day 0’; egg laying was monitored from the 2nd day post-eclosion.

Acknowledgements

We thank the Bloomington Drosophila Stock Center and the Vienna Drosophila RNAi center for fly stocks; Pierre Leopold for ILP antibodies; ARI and IISER (Pune) for use of the confocal microscopy facility; NCBS (Bangalore) and C-CAMP (Bangalore) for stocks; support from the National Facility for Gene Function in Health and Disease, IISER Pune for the IISER Drosophila facility; Gaiti Hasan and L. S. Shashidhara and Megha for helpful discussions; Bhagyashree Kaduskar for assistance with statistical analysis.

Competing interests

The authors declare no competing or financial interests.

Author contributions

Conceptualization and methodology : A.R.; Investigation: N.D., A.R., K.S.,S.T.; Formal analysis: N.D., A.R., K.S., S.T., G.D., G.S.R., Visualization : A.R.; Resources: A.R., G.S.R.; Supervision: A.R.; Data curation: N.D., A.R.; Writing original draft: A.R., G.D.; Writing review and editing: A.R., G.S.R and G.D; Project administration: A.R. and G.S.R; Funding acquisition: A.R., G.S.R.

Funding

Grant support from the Department of Biotechnology, Government of India to A.R. and G.S.R. (BT/PR23318/BRB/10/1597/2017); intramural support from the Agharkar Research Institute, Pune to A.R. and from IISER, Pune to G.S.R. G.D. is supported by a grant from the National Institutes of Health (HD093913). Deposited in PMC for release after 12 months.

Supplementary information

Supplementary information available online at http://dev.biologists.org/lookup/doi/10.1242/dev.166504.supplemental

References

Badisco, L., Van Wielendaele, P. and Vanden Broeck, J. (2013). Eat to reproduce: a key role for the insulin signaling pathway in adult insects. *Front. Physiol.* **4**, 202. doi:10.3389/fphys.2013.00202

Bai, H., Kang, P. and Tatar, M. (2012). Drosophila insulin-like peptide-6 (dilp6) expression from fat body extends lifespan and represses secretion of Drosophila insulin-like peptide-2 from the brain. *Aging Cell* **11**, 978-985. doi:10.1111/acel.12000

Boulan, L., Milan, M. and Leopold, P. (2015). The systemic control of growth. *Cold Spring Harb. Perspect. Biol.* **7**, a019117. doi:10.1101/cshperspect.a019117

Brogiolo, W., Stocker, H., Ikeya, T., Rintelen, F., Fernandez, R. and Hafen, E. (2001). An evolutionarily conserved function of the Drosophila insulin receptor and insulin-like peptides in growth control. *Curr. Biol.* **11**, 213-221. doi:10.1016/S0960-9822(01)00068-9

Broughton, S., Alic, N., Slack, C., Bass, T., Ikeya, T., Vinti, G., Tommasi, A. M., Driege, Y., Hafen, E. and Partridge, L. (2008). Reduction of DILP2 in Drosophila triages a metabolic phenotype from lifespan revealing redundancy and compensation among DILPs. *PLoS ONE* **3**, e3721. doi:10.1371/journal.pone.0003721

Burke, C. J., Huetteroth, W., Owald, D., Perisse, E., Krashes, M. J., Das, G., Gohl, D., Silies, M., Certel, S. and Waddell, S. (2012). Layered reward signalling through octopamine and dopamine in Drosophila. *Nature* **492**, 433-437. doi:10.1038/nature11614

Cao, C. and Brown, M. R. (2001). Localization of an insulin-like peptide in brains of two flies. *Cell Tissue Res.* **304**, 317-321. doi:10.1007/s004410100367

Deivasigamani, S., Basargekar, A., Shweta, K., Sonavane, P., Ratnaparkhi, G. S. and Ratnaparkhi, A. (2015). A presynaptic regulatory system acts transsynaptically via Mon1 to regulate glutamate receptor levels in Drosophila. *Genetics* **201**, 651-664. doi:10.1534/genetics.115.177402

Delanoue, R., Meschi, E., Agrawal, N., Mauri, A., Tsatskis, Y., McNeill, H. and Leopold, P. (2016). Drosophila insulin release is triggered by adipose Stunted ligand to brain Methuselah receptor. *Science* **353**, 1553-1556. doi:10.1126/science.aaf8430

Drummond-Barbosa, D. and Spradling, A. C. (2001). Stem cells and their progeny respond to nutritional changes during Drosophila oogenesis. *Dev. Biol.* **231**, 265-278. doi:10.1006/dbio.2000.0135

Enell, L. E., Kapan, N., Söderberg, J. A. E., Kahsai, L. and Nässel, D. R. (2010). Insulin signaling, lifespan and stress resistance are modulated by metabotropic GABA receptors on insulin producing cells in the brain of Drosophila. *PLoS ONE* **5**, e15780. doi:10.1371/journal.pone.0015780

Erion, R. and Sehgal, A. (2013). Regulation of insect behavior via the insulin-signaling pathway. *Front. Physiol.* **4**, 353. doi:10.3389/fphys.2013.00353

Erion, R., DiAngelo, J. R., Crocker, A. and Sehgal, A. (2012). Interaction between sleep and metabolism in Drosophila with altered octopamine signaling. *J. Biol. Chem.* **287**, 32406-32414. doi:10.1074/jbc.M112.360875

Feinberg, E. H., VanHoven, M. K., Bendesky, A., Wang, G., Fetter, R. D., Shen, K. and Bargmannl, C. I. (2008). GFP reconstitution across synaptic partners (GRASP) defines cell contacts and Synapses in living nervous systems. *Neuron* **57**, 353-363. doi:10.1016/j.neuron.2007.11.030

Gilbert, L. I., Serafin, R. B., Watkins, N. L. and Richard, D. S. (1998). Ecdysteroids regulate yolk protein uptake by Drosophila melanogaster oocytes. *J. Insect Physiol.* **44**, 637-644. doi:10.1016/S0022-1910(98)00020-1

Graham, P. and Pick, L. (2017). Drosophila as a model for diabetes and diseases of insulin resistance. *Curr. Top. Dev. Biol.* **121**, 397-419. doi:10.1016/bs.ctdb.2016.07.011

Grönke, S., Clarke, D.-F., Broughton, S., Andrews, T. D. and Partridge, L. (2010). Molecular evolution and functional characterization of Drosophila insulin-like peptides. *PLoS Genet.* **6**, e1000857. doi:10.1371/journal.pgen.1000857

Gruntenko, N. E. and Rauschenbach, I. Y. (2008). Interplay of JH, 20E and biogenic amines under normal and stress conditions and its effect on reproduction. *J. Insect Physiol.* **54**, 902-908. doi:10.1016/j.jinsphys.2008.04.004

Gruntenko, N. E. and Rauschenbach, I. Y. (2018). The role of insulin signalling in the endocrine stress response in Drosophila melanogaster: a mini-review. *Gen. Comp. Endocr.* **258**, 134-139. doi:10.1016/j.ygcen.2017.05.019

Gruntenko, N. E., Karpova, E. K., Adonyeva, N. V., Andreenkova, O. V., Burdina, E. V., Ilinsky, Y. Y., Bykov, R. A., Menshanov, P. N. and Rauschenbach, I. Y. (2019). Drosophila female fertility and juvenile hormone metabolism depends on the type of Wolbachia infection. *J. Exp. Biol.* **222**, jeb195347. doi:10.1242/jeb.195347

Hsu, H.-J. and Drummond-Barbosa, D. (2009). Insulin levels control female germline stem cell maintenance via the niche in Drosophila. *Proc. Natl. Acad. Sci. USA* **106**, 1117-1121. doi:10.1073/pnas.0809144106

Ikeya, T., Galic, M., Belawat, P., Nairz, K. and Hafen, E. (2002). Nutrient-dependent expression of insulin-like peptides from neuroendocrine cells in the CNS contributes to growth regulation in Drosophila. *Curr. Biol.* **12**, 1293-1300. doi:10.1016/S0960-9822(02)01043-6

Irizarry, J. and Stathopoulos, A. (2015). FGF signaling supports Drosophila fertility by regulating development of ovarian muscle tissues. *Dev. Biol.* **404**, 1-13. doi:10.1016/j.ydbio.2015.04.023

Kenyon, C. (2010). A pathway that links reproductive status to lifespan in Caenorhabditis elegans. *Ann. N. Y. Acad. Sci.* **1204**, 156-162. doi:10.1111/j.1749-6632.2010.05640.x
Kim, J., Zhao, T., Petralia, R. S., Yu, Y., Peng, H. C., Myers, E. and Magee, J. C. (2012). mGRASP enables mapping mammalian synaptic connectivity with light microscopy. *Nat. Methods* **9**, U96-U139. doi:10.1038/nmeth.1784
Knoblich, J. A. (2012). Asymmetric cell division and spindle orientation in neural stem cells - from Drosophila to humans. *Mol. Biol. Cell* **23**. doi:10.1016/j.exphem.2013.05.017
Kurz, C. L., Charroux, B., Chaduli, D., Viallat-Lieutaud, A. and Royet, J. (2017). Peptidoglycan sensing by octopaminergic neurons modulates Drosophila oviposition. *eLife* **6**, e21937. doi:10.7554/eLife.21937
LaFever, L. and Drummond-Barbosa, D. (2005). Direct control of germline stem cell division and cyst growth by neural insulin in Drosophila. *Science* **309**, 1071-1073. doi:10.1126/science.1111410
Lee, K.-S., Kwon, O.-Y., Lee, J. H., Kwon, K., Min, K.-J., Jung, S.-A., Kim, A.-K., You, K.-H., Tatar, M. and Yu, K. (2008). Drosophila short neuropeptide F signalling regulates growth by ERK-mediated insulin signalling. *Nat. Cell Biol.* **10**, 468-475. doi:10.1038/ncb1710
Li, L. and Xie, T. (2005). Stem cell niche: structure and function. *Annu. Rev. Cell Dev. Biol.* **21**, 605-631. doi:10.1146/annurev.cellbio.21.012704.131525
Lin, H. and Spradling, A. C. (1993). Germline stem cell division and egg chamber development in transplanted Drosophila germaria. *Dev. Biol.* **159**, 140-152. doi:10.1006/dbio.1993.1228
Luo, J., Lushchak, O. V., Goergen, P., Williams, M. J. and Nässel, D. R. (2014). Drosophila insulin-producing cells are differentially modulated by serotonin and octopamine receptors and affect social behavior. *PLoS ONE* **9**, e99732. doi:10.1371/journal.pone.0099732
Margolis, J. and Spradling, A. (1995). Identification and behavior of epithelial stem cells in the Drosophila ovary. *Development* **121**, 3797-3807.
Matova, N. and Cooley, L. (2001). Comparative aspects of animal oogenesis. *Dev. Biol.* **231**, 291-320. doi:10.1006/dbio.2000.0120
McLaughlin, J. M. and Bratu, D. P. (2015). Drosophila melanogaster oogenesis: an overview. *Methods Mol. Biol.* **1328**, 1-20. doi:10.1007/978-1-4939-2851-4_1
Mendes, C. C. and Mirth, C. K. (2016). Stage-specific plasticity in ovary size is regulated by insulin/insulin-like growth factor and ecdysone signaling in Drosophila. *Genetics* **202**, 703. doi:10.1534/genetics.115.179960
Middleton, C. A., Nongthomba, U., Parry, K., Sweeney, S. T., Sparrow, J. C. and Elliott, C. J. H. (2006). Neuromuscular organization and aminergic modulation of contractions in the Drosophila ovary. *BMC Biol.* **4**, 17. doi:10.1186/1741-7007-4-17
Mirth, C. K., Tang, H. Y., Makohon-Moore, S. C., Salhadar, S., Gokhale, R. H., Warner, R. D., Koyama, T., Riddiford, L. M. and Shingleton, A. W. (2014). Juvenile hormone regulates body size and perturbs insulin signaling in Drosophila. *Proc. Natl. Acad. Sci. USA* **111**, 7018-7023. doi:10.1073/pnas.1313058111
Nordmann, M., Cabrera, M., Perz, A., Bröcker, C., Ostrowicz, C., Engelbrecht-Vandré, S. and Ungermann, C. (2010). The Mon1-Ccz1 complex is the GEF of the late endosomal Rab7 homolog Ypt7. *Curr. Biol.* **20**, 1654-1659. doi:10.1016/j.cub.2010.08.002
Partridge, L., Alic, N., Bjedov, I. and Piper, M. D. W. (2011). Ageing in Drosophila: the role of the insulin/Igf and TOR signalling network. *Exp. Gerontol.* **46**, 376-381. doi:10.1016/j.exger.2010.09.003
Pauls, D., Blechschmidt, C., Frantzmann, F., el Jundi, B. and Selcho, M. (2018). A comprehensive anatomical map of the peripheral octopaminergic/tyraminergic system of Drosophila melanogaster. *Sci. Rep.* **8**, 15314. doi:10.1101/368803
Pfeiffer, B. D., Ngo, T.-T. B., Hibbard, K. L., Murphy, C., Jenett, A., Truman, J. W. and Rubin, G. M. (2010). Refinement of tools for targeted gene expression in Drosophila. *Genetics* **186**, 735-755. doi:10.1534/genetics.110.119917
Poteryaev, D., Datta, S., Ackema, K., Zerial, M. and Spang, A. (2010). Identification of the switch in early-to-late endosome transition. *Cell* **141**, 497-508. doi:10.1016/j.cell.2010.03.011
Rajan, A. and Perrimon, N. (2012). Drosophila cytokine unpaired 2 regulates physiological homeostasis by remotely controlling insulin secretion. *Cell* **151**, 123-137. doi:10.1016/j.cell.2012.08.019
Raushenbach, I. Y., Gruntenko, N. E., Bownes, M., Adonieva, N. V., Terashima, J., Karpova, E. K., Faddeeva, N. V. and Chentsova, N. A. (2004). The role of juvenile hormone in the control of reproductive function in Drosophila virilis under nutritional stress. *J. Insect Physiol.* **50**, 323-330. doi:10.1016/j.jinsphys.2004.02.001
Rauschenbach, I. Y., Karpova, E. K., Adonyeva, N. V., Andreenkova, O. V., Faddeeva, N. V., Burdina, E. V., Alekseev, A. A., Menshanov, P. N. and Gruntenko, N. E. (2014). Disruption of insulin signalling affects the neuroendocrine stress reaction in Drosophila females. *J. Exp. Biol.* **217**, 3733-3741. doi:10.1242/jeb.106815
Rezával, C., Nojima, T., Neville, M. C., Lin, A. C. and Goodwin, S. F. (2014). Sexually dimorphic octopaminergic neurons modulate female postmating behaviors in Drosophila. *Curr. Biol.* **24**, 725-730. doi:10.1016/j.cub.2013.12.051
Richard, D. S., Rybczynski, R., Wilson, T. G., Wang, Y., Wayne, M. L., Zhou, Y., Partridge, L. and Harshman, L. G. (2005). Insulin signaling is necessary for vitellogenesis in Drosophila melanogaster independent of the roles of juvenile hormone and ecdysteroids: female sterility of the chico1 insulin signaling mutation is autonomous to the ovary. *J. Insect Physiol.* **51**, 455-464. doi:10.1016/j.jinsphys.2004.12.013
Robinson, D. N. and Cooley, L. (1997). Genetic analysis of the actin cytoskeleton in the Drosophila ovary. *Annu. Rev. Cell Dev. Biol.* **13**, 147-170. doi:10.1146/annurev.cellbio.13.1.147
Roth, S. and Lynch, J. A. (2009). Symmetry breaking during Drosophila oogenesis. *Cold Spring Harb. Perspect. Biol.* **1**, a001891. doi:10.1101/cshperspect.a001891
Shim, J., Gururaja-Rao, S. and Banerjee, U. (2013). Nutritional regulation of stem and progenitor cells in Drosophila. *Development* **140**, 4647-4656. doi:10.1242/dev.079087
Spradling, A., Drummond-Barbosa, D. and Kai, T. (2001). Stem cells find their niche. *Nature* **414**, 98-104. doi:10.1038/35102160
Terashima, J. and Bownes, M. (2004). Translating available food into the number of eggs laid by Drosophila melanogaster. *Genetics* **167**, 1711-1719. doi:10.1534/genetics.103.024323
Ueishi, S., Shimizu, H. and Inoue, Y. H. (2009). Male Germline Stem Cell Division and Spermatocyte Growth Require Insulin Signaling in Drosophila. *Cell Struct. Funct.* **34**, 61-69. doi:10.1247/csf.08042
Wilson, T. G. (1982). A correlation between juvenile hormone deficiency and vitellogenic oocyte degeneration inDrosophila melanogaster. *Wilehm Roux Arch. Dev. Biol.* **191**, 257-263. doi:10.1007/BF00848413
Yousefian, J., Troost, T., Grawe, F., Sasamura, T., Fortini, M. and Klein, T. (2013). Dmon1 controls recruitment of Rab7 to maturing endosomes in Drosophila. *J. Cell Sci.* **126**, 1583-1594. doi:10.1242/jcs.114934
Zhou, C., Franconville, R., Vaughan, A. G., Robinett, C. C., Jayaraman, V. and Baker, B. S. (2015). Central neural circuitry mediating courtship song perception in male Drosophila. *Elife* **4**. doi:10.7554/eLife.08477

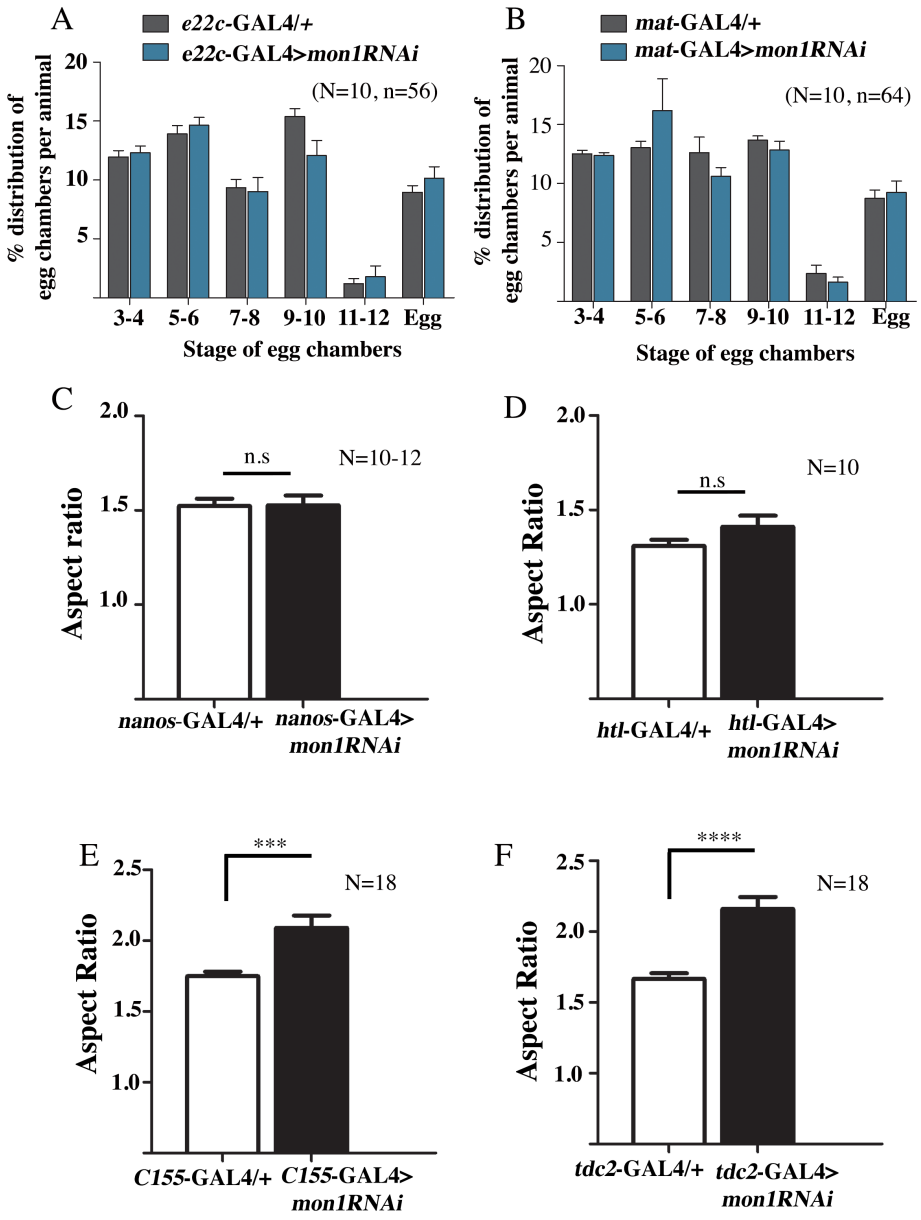

Figure {1: Knock-down of *mon1* activity in ovary associated tissue does not affect ovary size or egg chamber distribution.

(**A-B**) The distribution of egg chambers upon knock-down of *mon1* using *e22C*-GAL4 (A) and *mat*-GAL4 (B) is similar to their respective controls. (**C-D**) Knock-down of *mon1* using *nanos-GAL4* (C) or *htl* ^{GMR93H07}-GAL4 (D) does not change the aspect ratio of the ovaries compared to their respective controls. (*nanos*-GAL4/+: 1.52-±0.04 (n=12 ovaries) and *nanos*-GAL4>*UAS-mon1RNAi*: 1.52-±0.05 (n=11 ovaries; *htl* ^{GMR93H07}-GAL4/+: 1.31±0.03 (n=10 ovaries) and *htl* ^{GMR93H07}-GAL4> *UAS-mon1RNAi: 1.41-±0.05* (n=10 ovaries)). (**E-F**) Compared to their respective controls, downregulation of *mon1* using either *C155*-GAL4 **(**E) or *tdc2*-GAL4 (F) leads to decrease in ovary size evident from the increase in aspect ratio in these animals. (C155-GAL4/+: 1.75±0.03 (n=18) ovaries and C155-GAL4> *UAS-mon1RNAi*: 2.09±0.08 (n=18 ovaries)) ; (*tdc2*-GAL4/+: 1.66±0.04 (n-18 ovaries) and *tdc2*-GAL4> *UAS-mon1RNAi*: 2.15±0.08 (n=20 ovaries)). **** indicates p<0.0001, *** indicates p<0.001, Students t-test.

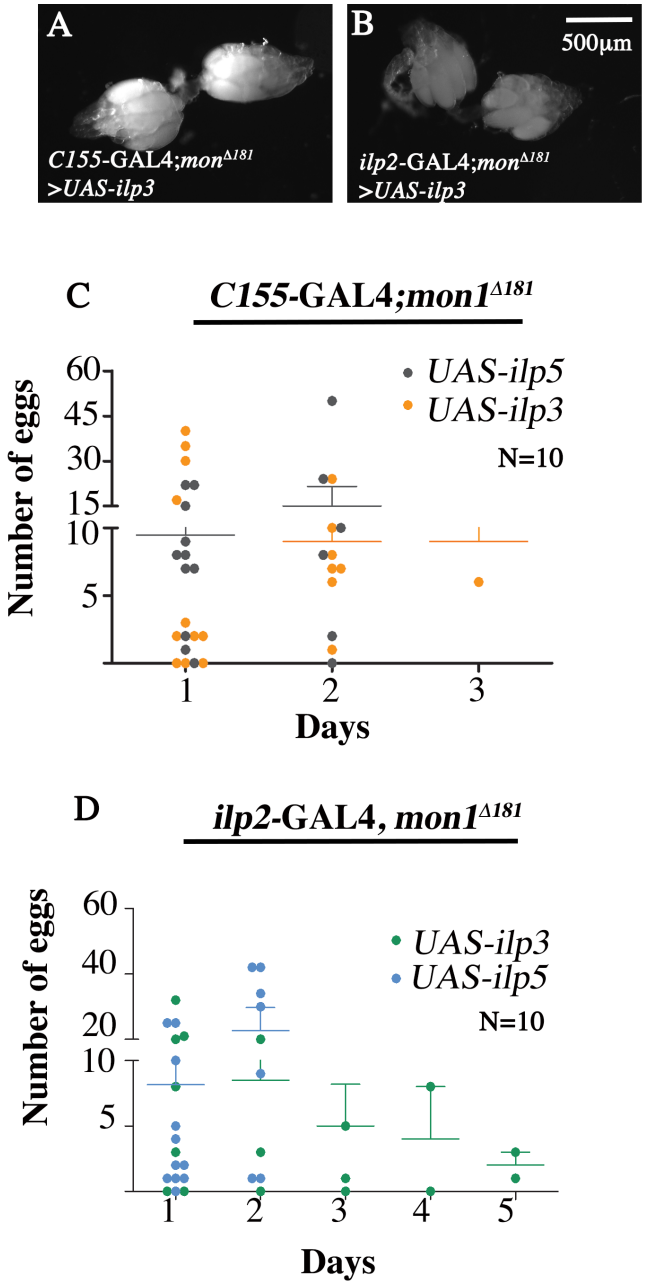

Figure {2: Pan-neuronal and IPC specific expression of *UAS-ilp5* and *UAS-ilp3* rescues fecundity in *mon1*$^{\Delta 181}$ mutants.

(A-B) Ovary from *C155-GAL4; mon1*$^{\Delta 181}$*>UAS-ilp3* (A) and *ilp2*-GAL4; *mon1*$^{\Delta 181}$*>UAS-ilp3* (B). Note presence of eggs when *ilp3* is expressed in neurons.

(C-D) Comparison of the eggs laid by *C155-GAL4; mon1*$^{\Delta 181}$*>UAS-ilp5* and *C155-GAL4; mon1*$^{\Delta 181}$*> UAS-ilp3* (C) shows no significant difference in the fecundity of these animals. Both genotypes appear to be equivalent in their ability to lay eggs. A similar 'rescue' of fecundity was observed upon expression of *ilp5* and *ilp3* in IPCs (D). The ability to lay eggs is significantly better than that of *mon1*$^{\Delta 181}$ homozygous females, which do not lay eggs but below (1/5th) the ability of wild type animals that lay approximately 60-80 eggs per day.

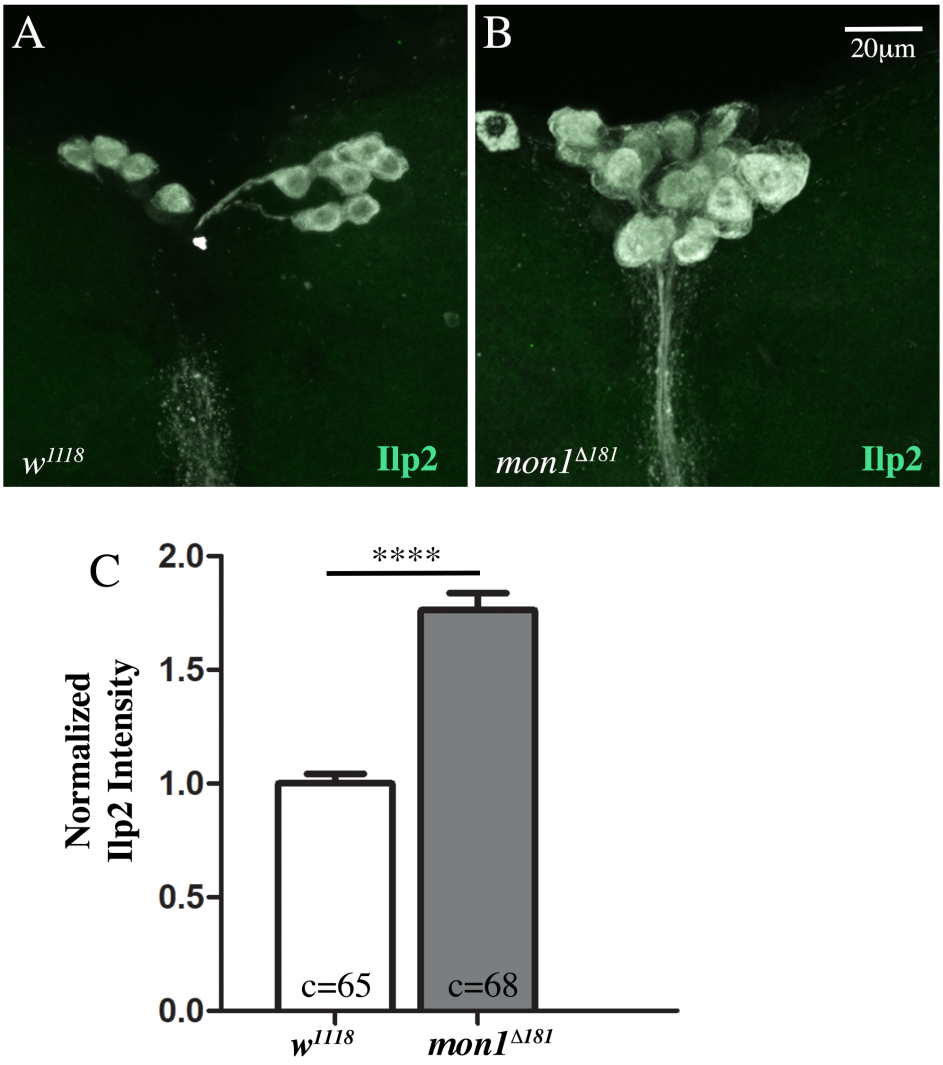

Figure S3: IPCs show increase in Ilp2 levels in *mon1*$^{\Delta 181}$ mutants.
(A-B) Adult brains of wildtype (w^{1118}) and *mon1*$^{\Delta 181}$ mutants stained with anti-Ilp2. Mutants show a significant increase in Ilp2 staining. **(C)** Quantification of the intensity in IPC cell bodies shows ~ 70% increase in Ilp2 levels in *mon1*$^{\Delta 181}$ (1.0±0.042 (wildtype, n= 65 cells) versus 1.76-±0.07 (*mon1*$^{\Delta 181}$, n=68)). **** indicates p<0.0001, Students t-test. c=number of cell bodies counted for image analysis.

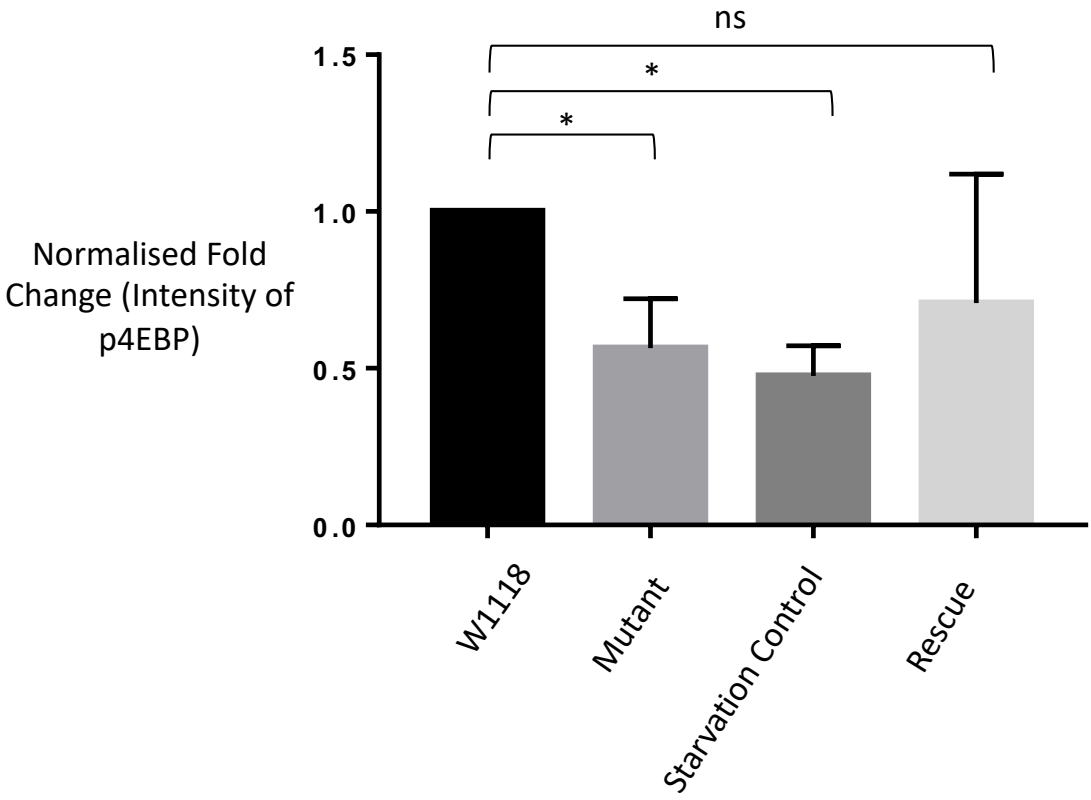

Figure S4: Measurement of phosphorylated-4EBP1 levels in whole animal extracts.
Normalized fold intensity for phospho-4EBP1 (Cell Signaling, Thr(37/46), 236B4, Rb mAb #2855) intensity on Western blots indicating reduction of 45% in whole animal extracts. N=3, n (number of flies)=4. 1 way ANOVA. Error bars represent standard error. *, $p<0.05$.

Two day old adults were homogenized in 1X RIPA buffer (150 mM NaCl, 0.1% NP40, 0.5% DOC, 25 mM Tris pH 7.4) with phosphatase inhibitors, the protein concentration measured (see below) and equal concentrations of protein loaded for w^{1118}, *mon1* mutant, *Starved-*w^{1118} and animals 'rescued' by expression Mon1 in OPN neurons (*tdc2-GAL4>UAS-mon1:HA*).
Total protein concentration was measured using a detergent compatible BCA protein assay kit (Pierce, #23225). Average protein concentration estimated per animal was 2.03 mg for w^{1118} (fed), 1.80 for w^{1118} (starved) and 1.89 for *mon1* mutant.